AD-A116 882 OHIO STATE UNIV COLUMBUS ELECTROSCIENCE LAB F/G 17/3
A PROPOSED DIRECTION FINDING AND POLARIZATION SENSING SCHEME.(U)
MAR 76 E P EKELMAN, G A THIELE N00140-75-C-6116
UNCLASSIFIED ESL-4111-3 NL

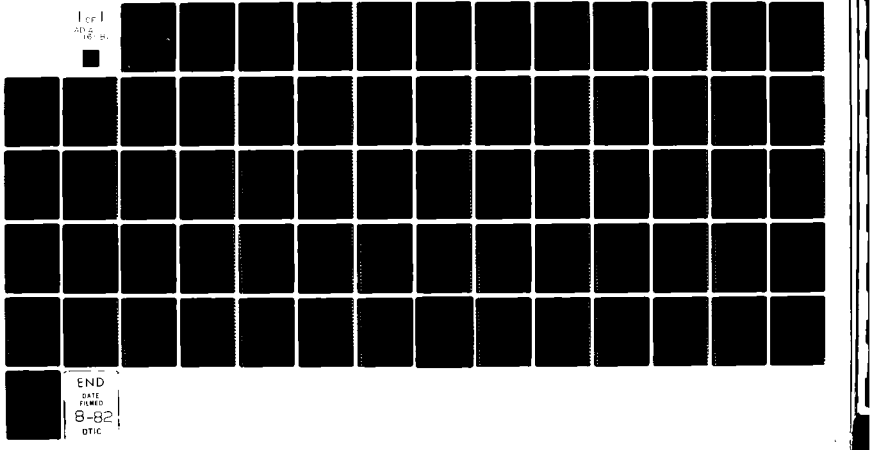

END
DATE FILMED
8-82
DTIC

(2)

[illegible]

Ernest F. Ekelb[illegible] Jr. and Gary F. Thiele

The Ohio State University

[illegible]

Department of Electrical Engineering
Columbus, Ohio [illegible]

TECHNICAL REPORT [illegible]-3

March 1976

Contract N00140-76-C-6116

Approved for public release; distribution unlimited.

Naval Regional Procurement Office
Philadelphia, Newport Division, Building No. 132
[illegible]

NOTICES

[illegible] and are used for any purpose other than in connection with a definitely related government procurement operation, the United States Government thereby incurs no responsibility nor any obligation whatsoever, and the fact that the Government may have formulated, furnished, or in any way supplied the said drawings, specifications, or other data, is not to be regarded by implication or otherwise as in any manner licensing the holder or any other person or corporation, or conveying any rights or permission to manufacture, use, or sell any patented invention that may in any way be related thereto.

UNCLASSIFIED

SECURITY CLASSIFICATION OF THIS PAGE (When Data Entered)

REPORT DOCUMENTATION PAGE	READ INSTRUCTIONS BEFORE COMPLETING FORM
1. REPORT NUMBER	2. GOVT ACCESSION NO. ADA116882	3. RECIPIENT'S CATALOG NUMBER
4. TITLE (and Subtitle) A PROPOSED DIRECTION FINDING AND POLARIZATION SENSING SCHEME	5. TYPE OF REPORT & PERIOD COVERED Technical Report
	6. PERFORMING ORG. REPORT NUMBER ESL 4111-3
7. AUTHOR(s) Ernest P. Ekelman, Jr. and Gary A. Thiele	8. CONTRACT OR GRANT NUMBER(s) N00140-75-C-6116
9. PERFORMING ORGANIZATION NAME AND ADDRESS The Ohio State University ElectroScience Laboratory, Department of Electrical Engineering Columbus, Ohio 43212	10. PROGRAM ELEMENT, PROJECT, TASK AREA & WORK UNIT NUMBERS
11. CONTROLLING OFFICE NAME AND ADDRESS Naval Regional Procurement Office Philadelphia, Newport Division Building No. 132 Newport, Rhode Island 02840	12. REPORT DATE March 1976
	13. NUMBER OF PAGES 63
14. MONITORING AGENCY NAME & ADDRESS(if different from Controlling Office)	15. SECURITY CLASS. (of this report) UNCLASSIFIED
	15a. DECLASSIFICATION/DOWNGRADING SCHEDULE

16. DISTRIBUTION STATEMENT (of this Report)

Approved for public release; distribution unlimited.

17. DISTRIBUTION STATEMENT (of the abstract entered in Block 20, if different from Report)

18. SUPPLEMENTARY NOTES

19. KEY WORDS (Continue on reverse side if necessary and identify by block number)

Direction-finding
Polarization-sensing
Small antenna array

20. ABSTRACT (Continue on reverse side if necessary and identify by block number)

This report proposes and demonstrates a direction finding scheme utilizing an array of electrically small antenna elements located on a metallic circular cylinder of modest electrical size. The investigation was accomplished with the aid of a digital computer and two numerical techniques for analyzing electromagnetic radiation problems. By correctly combining the inputs of properly oriented radiators, a system is demonstrated that is

DD FORM 1 JAN 73 1473 EDITION OF 1 NOV 65 IS OBSOLETE

UNCLASSIFIED

SECURITY CLASSIFICATION OF THIS PAGE (When Data Entered)

20.

capable of angle-of-arrival determination over a frequency band with simple signal processing when the frequency, phase, and polarization of the incident signal are unknown.

ACKNOWLEDGEMENTS

I would like to acknowledge the continuous help and guidance provided by my advisor Gary A. Thiele throughout the period of investigation and preparation of this report. I would also like to thank J. H. Richmond, W. D. Burnside, and N. N. Wang for their numerous discussions and consultations. Special credit is given to E. Burvin for the tapered loading scheme discussed in Section F of Chapter IV.

The work reported in this report was also used as a thesis submitted to The Ohio State University, Department of Electrical Engineering as partial fulfillment for the degree Master of Science.

CONTENTS

CHAPTER I

INTRODUCTION

Electrically small antennas have been the subject of a great deal of research because of their importance to communication systems. For many reasons, it is often impractical to use an electrically large antenna which has characteristics desirable for many applications. So the necessary electrically small antenna often becomes the limiting factor in the capability of a communication system. The subject of this investigation is the use of electrically small antennas in a direction finding system.

The problem that is addressed can be defined by enumerating the physical constraints and generally desirable characteristics of the system. The antenna radiating elements or array are to be electrically small; that is, less than a wavelength in extent and must operate on or very near a metallic support cylinder of modest electric size. These geometrical specifications make the problem a conformal array type. The system is to perform over a broad frequency band. The antenna elements are to remain mechanically stationary and electrically passive. Signal processing is to be simple; that is, the receiver is capable of only minimal signal manipulation. Azimuthal direction of the incoming signal is to be found without knowing the frequency, phase, or polarization of the signal. The constraints do not completely specify any particular direction finding system, but they do characterize a general class of systems.

The investigation described herein was accomplished with the aid of a digital computer and two approximate techniques of solving electromagnetic radiation problems. Chapter II briefly presents the concept behind the piecewise-sinusoidal reaction matching technique. Chapter III shows the development of a hybrid method which uses modal solutions for an infinite cylinder. The research was conducted by modeling various electrically small radiators on the cylinder and analyzing the structures with the methods of Chapters II and III for the purpose of investigating the direction scheme of Chapter IV.

The main contribution of this thesis is the direction finding scheme discussed in Chapter IV. Thus, Chapter IV develops the proposed direction finding system by discussing the consequences of the constraints and presenting results for a particular radiator. Results of this radiator demonstrate the method which uses electrically small elements forming an array around the cylinder that is capable of angle of arrival determination over a frequency band with minimal signal processing when the frequency, phase, and polarization of the signal are unknown.

CHAPTER II

SINUSOIDAL REACTION TECHNIQUE

A. Introduction

Solutions of electromagnetic radiation problems are, except for simple geometries, only possible through approximations. A recent and very successful approximation method involves modeling antennas or scatterers by thin-wire grids. A computer program for thin-wire structures in a homogeneous conducting medium has been published by Richmond [1]. This program was adopted and used extensively to analyze the various antenna structures investigated. The program is a specialization of the Method of Moments. This chapter will briefly discuss the concepts behind the program and then present some results for simple radiators in the presence of a finite length cylinder.

B. Method of Moments

Electromagnetic radiation problems can be represented by integral equations containing field terms and appropriate inhomogeneous source terms, either actual or equivalent. The equations seldom lead to tractable closed-form analytic solutions. The Method of Moments, however, is a general approach which essentially reduces the integral equation to a system of linear algebraic equations with unknown coefficients related to an expansion of a current distribution.

Consider a perfectly-conducting body with surface current density $\underline{J}_{EQ}$ induced on it. Applying boundary conditions at the surface of the conductor gives for the total electric field

$$\underline{E}_{tan} = 0 = \underline{E}^{s}_{tan} + \underline{E}^{i}_{tan} \tag{2-1}$$

where $\underline{E}^{i}_{tan}$ is the tangential component of the incident electric field and $\underline{E}^{s}_{tan}$ is the scattered electric field radiated by the equivalent current density $\underline{J}_{EQ}$. The subscript tan will be dropped with the understanding that the fields are the tangential components, so Eq. (2-1) becomes

$$-\underline{E}^{s} = \underline{E}^{i} \quad . \tag{2-2}$$

To relate the equivalent current density $\underline{J}_{EQ}$ to the scattered electric field $\underline{E}^s$, a linear operator L is defined

$$L(\underline{J}_{EQ}) = -\underline{E}^s \tag{2-3}$$

where the concepts of linear spaces and operators are used. Thus, Eqs. (2-2) and (2-3) give

$$L(\underline{J}_{EQ}) = \underline{E}^i \quad . \tag{2-4}$$

For a typical electromagnetic radiation problem $\underline{E}^i$ is a known source and $\underline{J}_{EQ}$ is the unknown response to be determined. L will be an integral operator which operates on a unique $\underline{J}_{EQ}$ to give the known excitation. That is, L^{-1} exists such that

$$\underline{J}_{EQ} = L^{-1}(\underline{E}^i) \quad . \tag{2-5}$$

For a given problem the domain of the operator must be defined by determining the space of functions $\underline{J}_{EQ}$ on which it operates with the resulting functions forming the range of the operator. The operator L can be considered as the transformation mapping from a subset containing $\underline{J}_{EQ}$ to one containing $\underline{E}^i$. Besides determining the range and domain of the operator, it is necessary to formulate an inner product $\langle \underline{J},\underline{E} \rangle$, which is a scalar called reaction. The inner product is defined such that it forms a unitary space. The following axioms are satisfied:

$$\langle \underline{J},\underline{E} \rangle = \langle \underline{E},\underline{J} \rangle \tag{2-6}$$

$$\langle \alpha\underline{J} + \beta\underline{J},\underline{E} \rangle = \alpha\langle \underline{J},\underline{E} \rangle + \beta\langle \underline{J},\underline{E} \rangle \tag{2-7}$$

If $\langle \underline{J}^*,\underline{J} \rangle > 0$, then $\underline{J} \neq 0$ (2-8)

If $\langle \underline{J}^*,\underline{J} \rangle = 0$, then $\underline{J} = 0$ (2-9)

where α and β are scalars and * denotes complex conjugation. The solution to Eq. (2-5) follows from the four-step procedure:

1. Expand the unknown in a series of basis functions, $\underline{J}_m$ spanning $\underline{J}_{EQ}$ in the domain of L.

2. Determine a suitable inner product and define a set of weighting functions.

3. Take the inner product and thereby form the matrix equation.

4. Solve the matrix equation for the unknowns.

Once the unknown current coefficients are obtained, the radiation characteristics such as far-field patterns and impedance are easily obtained.

A specialization of this general Method of Moments which is particularly convenient for electromagnetic radiation problems is Galerkin's Method. Thus, step (1) requires the expansion of the unknown $\underline{J}_{EQ}$ in a series of basis functions $\underline{J}_1, \underline{J}_2, \underline{J}_3 \ldots \underline{J}_m$ on the surface of the conducting body and spanning the domain of L. $\underline{J}_{EQ}$ can be represented as

$$\underline{J}_{EQ} = \sum_m I_m \underline{J}_m \tag{2-10}$$

where I_m's are the desired unknown complex current coefficients. Substituting Eq. (2-10) into Eq. (2-4) gives

$$L \left(\sum_m I_m \underline{J}_m \right) = \underline{E}^i \tag{2-11}$$

which is

$$\sum_m I_m L(\underline{J}_m) = \underline{E}^i \tag{2-12}$$

by the linearity of L.

Step (2) defines a set of weighting functions $\underline{W}_1, \underline{W}_2, \cdots \underline{W}_n$ in the domain of L and forms the inner product

$$\sum_m I_m \langle \underline{W}_n, L(\underline{J}_m) \rangle = \langle \underline{W}_n, \underline{E}^i \rangle \quad . \tag{2-13}$$

Galerkin's specialization is that the weighting functions are chosen equal to the expansion functions, that is, $\underline{W}_m = \underline{J}_m$. Thus, Eq. (2-13) becomes

$$\sum_m I_m \langle \underline{J}_n, L(\underline{J}_m) \rangle = \langle \underline{J}_n, \underline{E}^i \rangle \tag{2-14}$$

where the inner products are identified as reactions.

Step (3) calculates the various inner products which may be represented in matrix form:

$$\begin{bmatrix} \langle \underline{J}_1, L(\underline{J}_1)\rangle & \langle \underline{J}_1, L(\underline{J}_2)\rangle & \cdots & \langle \underline{J}_1, L(\underline{J}_m)\rangle \\ \langle \underline{J}_2, L(\underline{J}_1)\rangle & \langle \underline{J}_2, L(\underline{J}_2)\rangle & \cdots & \langle \underline{J}_2, L(\underline{J}_m)\rangle \\ \vdots & \vdots & & \vdots \\ \langle \underline{J}_m, L(\underline{J}_1)\rangle & \langle \underline{J}_m, L(\underline{J}_2)\rangle & \cdots & \langle \underline{J}_m, L(\underline{J}_m)\rangle \end{bmatrix} \begin{bmatrix} I_1 \\ I_2 \\ \vdots \\ I_m \end{bmatrix} = \begin{bmatrix} \langle \underline{J}_1, \underline{E}^i\rangle \\ \langle \underline{J}_2, \underline{E}^i\rangle \\ \vdots \\ \langle \underline{J}_m, \underline{E}^i\rangle \end{bmatrix} \tag{2-15}$$

This may be written in compact notation

$$[Z]\ (I) = (V) \tag{2-16}$$

where the elements are considered as generalized impedances, currents and voltages, respectively.

Step (4) involves standard matrix inversion techniques to solve for the current column. The simple notation used to represent this general moment method formulation makes the solution appear deceptively simple. Each of the m^2 impedance elements in Eq. (2-15) suggests at least two integrations, one when applying the integral operator and the second dictated by the inner product. The next section discusses a method which is particularly efficient when applied to thin wire solutions that can be used, for example, in wire-grid modeling.

C. The Piecewise-Sinusoidal Basis: Reaction-Matching

In this section, the method [2] of choosing piecewise-sinusoidal basis functions to obtain the elements of the impedance matrix [Z] using the reaction concept will be outlined. The reaction concept is also called reaction-matching and can be demonstrated by examining a dipole antenna with a test source placed at the center. For the linear antenna $\underline{J}^i$ and $\underline{M}^i$, the original sources may be replaced with

$$\underline{J}_{EQ} = \hat{n} \times \underline{H} \tag{2-17}$$

and

$$\underline{M}_{EQ} = \underline{E} \times \hat{n} \tag{2-18}$$

on the closed surface of the dipole. By the equivalence principle $\underline{J}_{EQ}$ and $\underline{M}_{EQ}$ on the surface generate the fields $\underline{E}$ and $\underline{H}$ outside the dipole surface. The dipole is perfectly conducting so $\underline{M}_{EQ}$ vanishes on the surface. Next, a filamentary electric line test source is placed inside the dipole coincident with its axis. This test source is reacted with the equivalent surface source of $\underline{E}$ and $\underline{H}$. Using the term "react" implies the application of the reciprocity theorem,

$$\langle a,b \rangle = \int\int\int_{V_a} [\underline{J}(a) \cdot \underline{E}(b) - \underline{M}(a) \cdot \underline{H}(b)] \, d V_a \quad . \tag{2-19}$$

Here $\underline{J}(a)$ and $\underline{M}(a)$ are the test source distributions generating $E(a)$ and $H(a)$ in the presence of b, the equivalent sources. Reaction then is a measure of the coupling between the two sources a and b. The equivalent surface current density $\underline{J}_{EQ}$ can be represented by an equivalent filamentary source parallel to the test source and displaced by the radius of the dipole.

Assuming a piecewise-sinusoidal current distribution on the filamentary test source

$$I_t (z) = \frac{\sin k (h - |z|)}{\sin k h} \tag{2-20}$$

where the z-oriented source has length 2h, z is measured from the coordinate origin and source center, and $k = 2\pi/\lambda$. The current on the equivalent source is expressed as

$$I (z) = I_1 \frac{\sin k (h - |z|)}{\sin k h} \tag{2-21}$$

where I_1 is the desired unknown current coefficient caused by generator voltage V_1. By the reciprocity theorem, the solution is found from $I_1 Z = V_1$ where Z is the reaction between the test source with known field $\underline{E}_t$ and $\underline{H}_t$ and the equivalent source $\underline{J}_{EQ}$ of the true fields $\underline{E}$ and $\underline{H}$.

$$Z = \frac{V_1}{I_1} = \frac{1}{I_1} \oint_s \underline{J}_{EQ} \cdot \underline{E}_t \, ds \tag{2-22}$$

This concept of a test source with a piecewise-sinusoidal current distribution with known field being reacted with the equivalent true source distribution on the surface of a radiator is expanded

to generate an impedance matrix from which the unknown current coefficients are calculated. Consider, for example, a circular loop antenna which may be modeled by a polygon of thin wires forming a tubular surface. A filamentary dipole is placed in the center of and coincident with two segments of the polygon. Reciprocity is enforced successively between the test dipole and each of the tubular-surface dipoles in turn, thus generating one row of the impedance matrix. The test source is then moved around the loop to create the other rows. Relating this back to the general Method of Moments, it is seen that the integral operator and inner product have been defined by the reaction integral Eq. (2-19). The expansion and weighting functions are the piecewise-sinusoidal functions making this a form of Galerkin's method. Thiele [3] has discussed the advantages of this reaction-matching technique in terms of accuracy and rate of convergence over other methods.

D. Calculation of Antenna Characteristics

Once the current is known on the perfectly-conducting body, that is, the antenna structure, calculation of other antenna characteristics follow directly. The current distribution for the piecewise-sinusoidal functions will simply be the superposition of all the equivalent tubular dipole currents defined at various points along the antenna. Once the terminal currents are known, the terminal impedance follows from

$$Z_t = V_t / I_t \tag{2-23}$$

where V_t is the terminal voltage. Lumped loading may be included by adding the load terms to the appropriate elements of the impedance matrix.

To calculate the far field anywhere in space due to a known current is straightforward. For a filamentary source

$$\underline{E}(r,\theta,\phi) = - j\omega\mu \frac{e^{-jkr_o}}{4\pi r_o} \int_{\substack{\text{along} \\ \text{the wire} \\ \text{antenna}}} \underline{I}(\tau)\, F(\theta,\phi)\, d\tau \tag{2-24}$$

where

$$F(\theta,\phi) = \text{EXP}\ jk[x' \sin\theta \cos\phi + y' \sin\theta \sin\phi + z' \cos\theta]$$

and (x', y', z') denotes the source coordinates while (θ,ϕ) denotes

the observation point in the far field. The above equation must be applied at points over the entire antenna structure and the results superimposed to give the total far-field $E_\theta(r,\theta,\phi)$ and $E_\phi(r,\theta,\phi)$.

The power gain is determined by

$$G(\theta,\phi) = \frac{[\,|E_\theta|^2 + |E_\phi|^2\,]\, r_o^2}{30\,|I_t|^2\, R_t} \qquad (2\text{-}25)$$

where R_t is the real part of the antenna terminal impedance.

Determination of the radiation efficiency requires calculating the input and radiated powers. The time average power input is

$$P_{in} = |I_t|^2\, R_t \quad . \qquad (2\text{-}26)$$

The radiated power is

$$P_r = |I_t|^2\, R_r \qquad (2\text{-}27)$$

where R_r is the radiation resistance which, for the lossless perfectly-conducting case, is equal to R_t. The radiation efficiency is then defined as

$$\frac{P_r}{P_{in}} = \frac{|I_t|^2\, R_r}{|I_t|^2\, R_t} = \frac{R_r}{R_t} \quad . \qquad (2\text{-}28)$$

E. Thin-Wire Modeling

The concept discussed in this section is the application of the sinusoidal reaction technique to not only the antenna but also to the metallic environment or support structure of the antenna. The surfaces of metal bodies are modeled by a system or grid of wire segments. The resulting generalized polygon obtained with this modeling technique essentially has the capability of representing a surface of arbitrary shape. The only practical limitation of the wire-grid modeling procedure is the size of the impedance matrix [Z] which must be solved. The matrix size is directly related to the electrical size of the surface area that must be modeled.

Two important examples using this technique will now be presented, the results of which will be referred to throughout this text. Consider a perfectly-conducting circular cylinder of finite length with first a radial monopole attached and second, a dipole element located near the cylinder and oriented coaxial to it. The radiators are modeled with consecutive straight wire segments while the cylinder is modeled with connected hexagons. Figure 2-1 shows the configuration with dimensions and orientations. This investigation is concerned with results over a frequency range. To accomplish this, the physical dimensions of the model are held constant, while the frequency and, correspondingly, the electrical dimensions are varied. The computer program accepts as input the locations of all points which are the vertices of the segments formed by connecting the points, the conductivity and diameter of the wires, and the frequency of operation.

The program first sorts the segments and forms the needed number of modes. Next, the impedance matrix is calculated by assuming piecewise-sinusoidal currents as test sources inside the wires and as the basis functions on the wire surfaces and then enforces the reaction relationships between them. The symmetric properties of the matrix are used to reduce storage and running time. The matrix is inverted and the simultaneous algebraic equations are solved for the unknown complex current coefficients. As the previous section demonstrated, the desired antenna characteristics follow directly from this point. Figures 2-2 and 2-3 show the far-field patterns decomposed into phi and theta components for a representative frequency in the two principal planes for first the radial monopole and then the axial dipole.

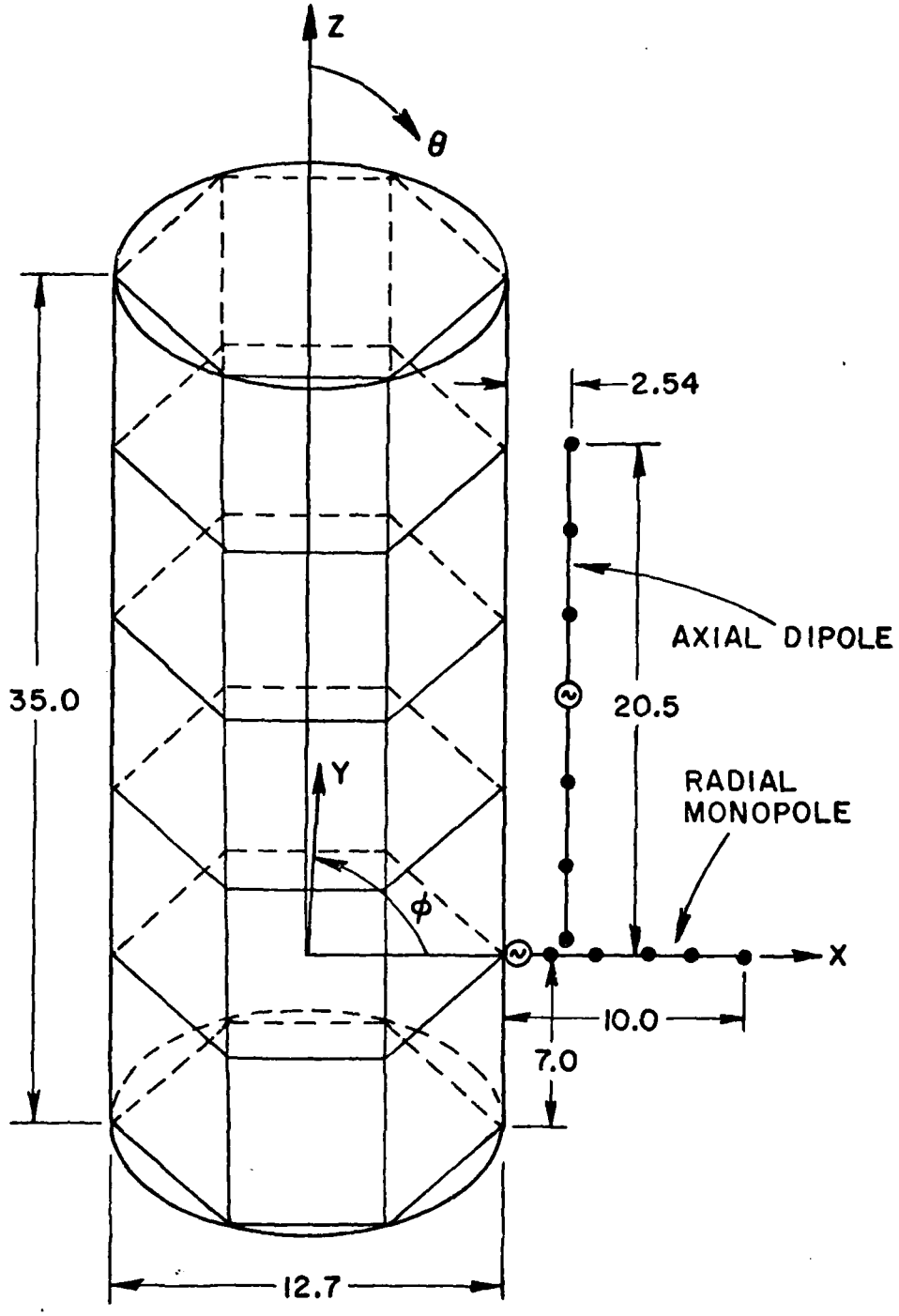

Fig. 2-1. Wire grid model of circular cylinder with a radial monopole or an axial dipole. The orientation and coordinate system is the one used for the patterns. The dimensions are in centimeters.

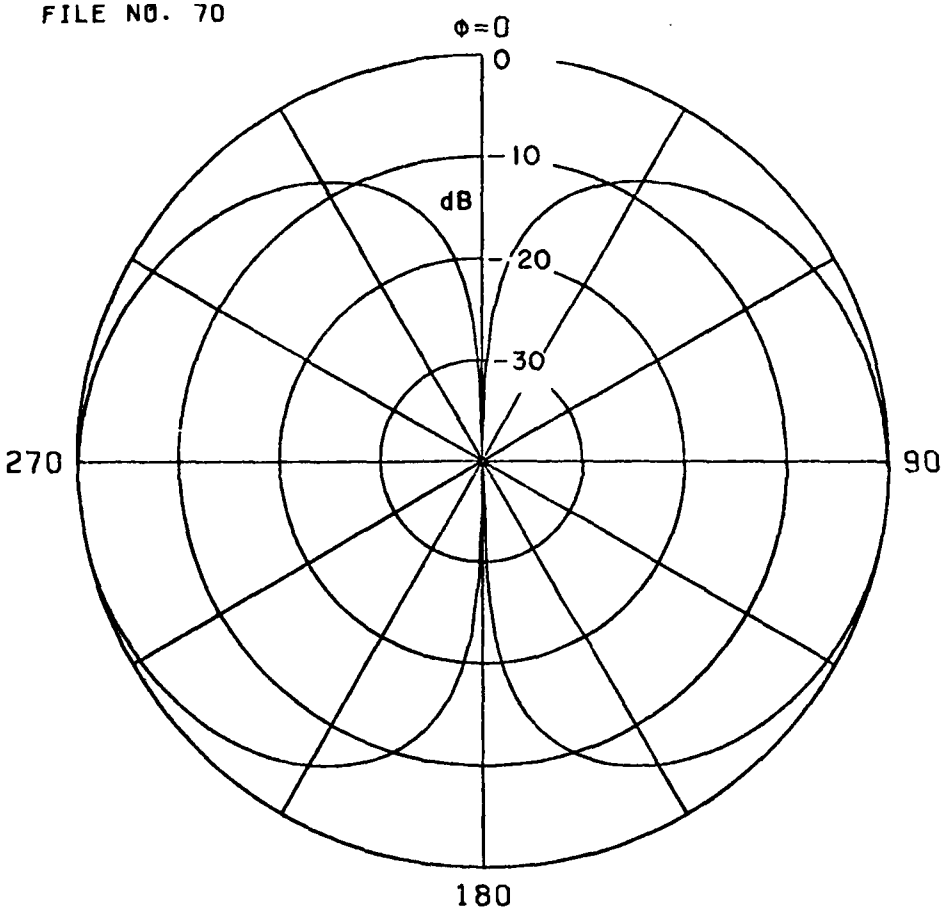

Fig. 2-2(a). Phi component of the far electric field pattern in the horizontal plane for the radial monopole of Fig. 2-1 located on the finite length cylinder.

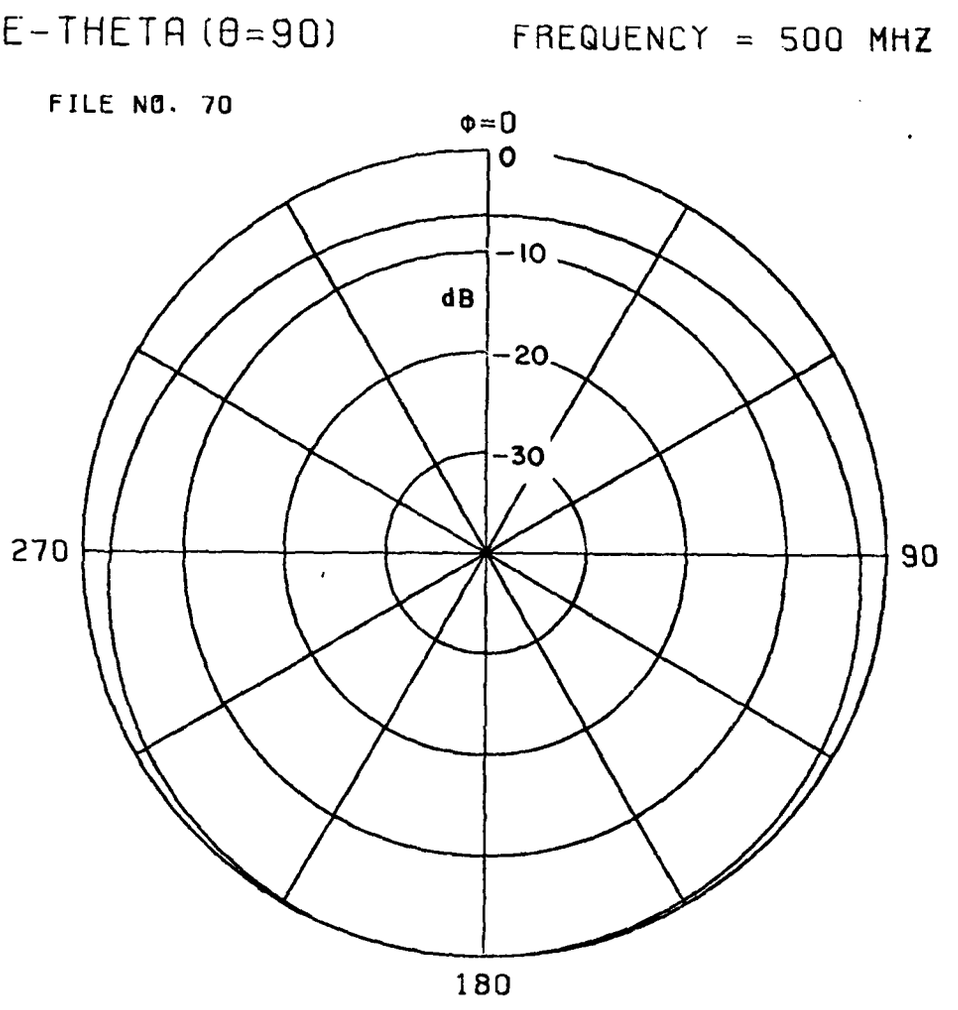

Fig. 2-2(b). Theta component of the far electric field pattern in the horizontal plane for the radial monopole of Fig. 2-1 located on the finite length cylinder.

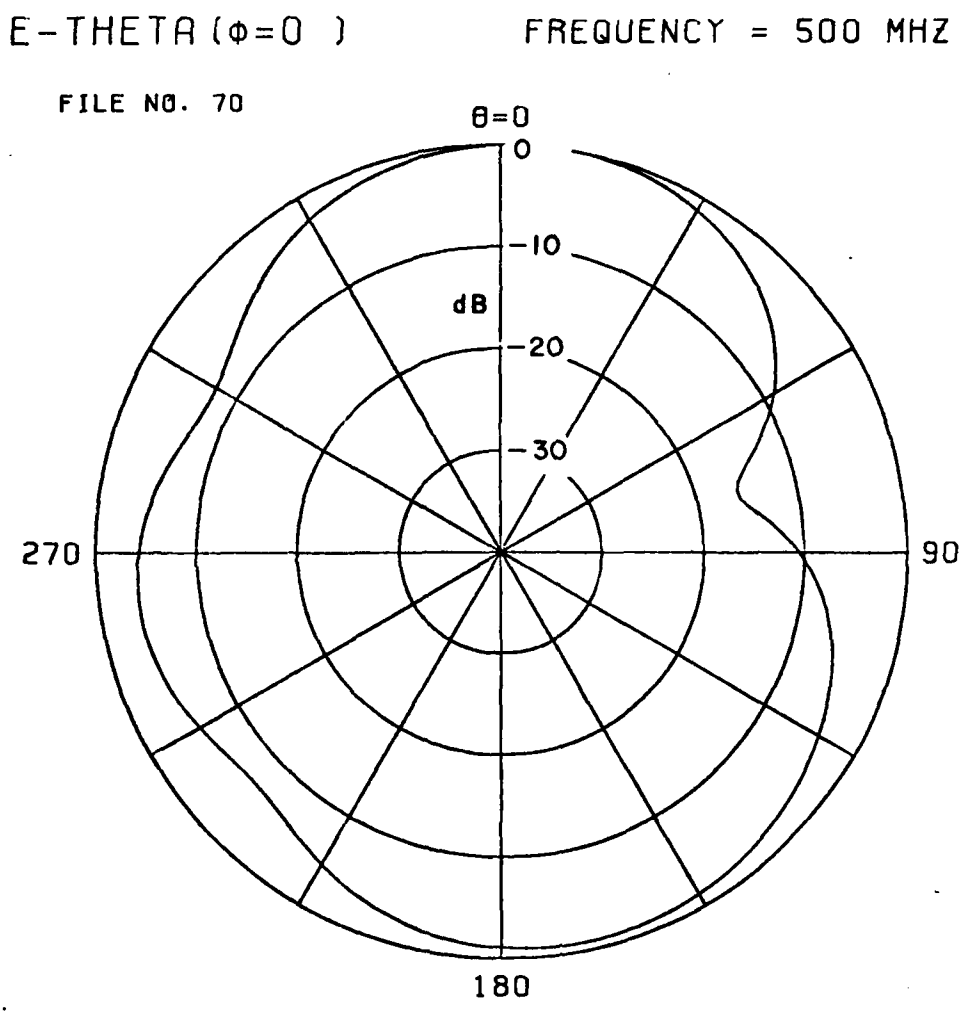

Fig. 2-2(c). Theta component of the far electric field pattern in the vertical plane for the radial monopole of Fig. 2-1 located on the finite length cylinder.

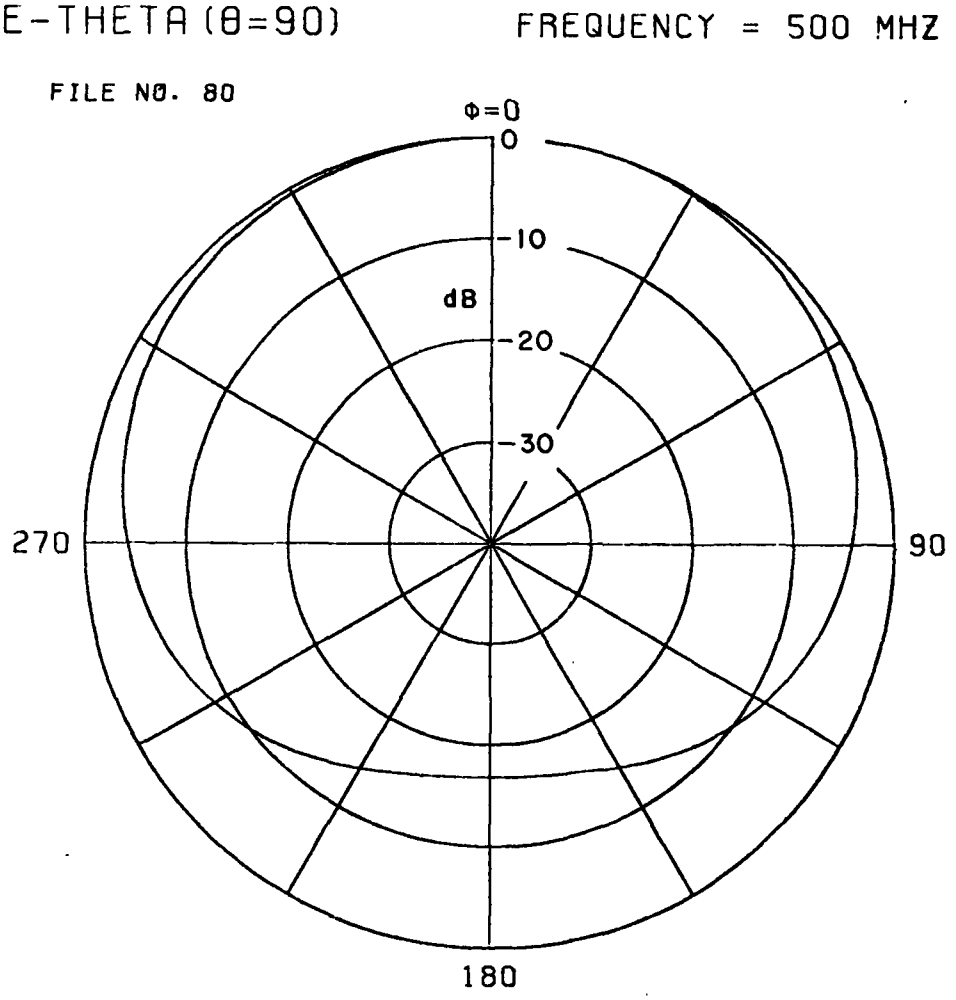

Fig. 2-3(a). Theta component of the far electric field pattern in the horizontal plane for the axial dipole of Fig. 2-1 located on the finite length cylinder.

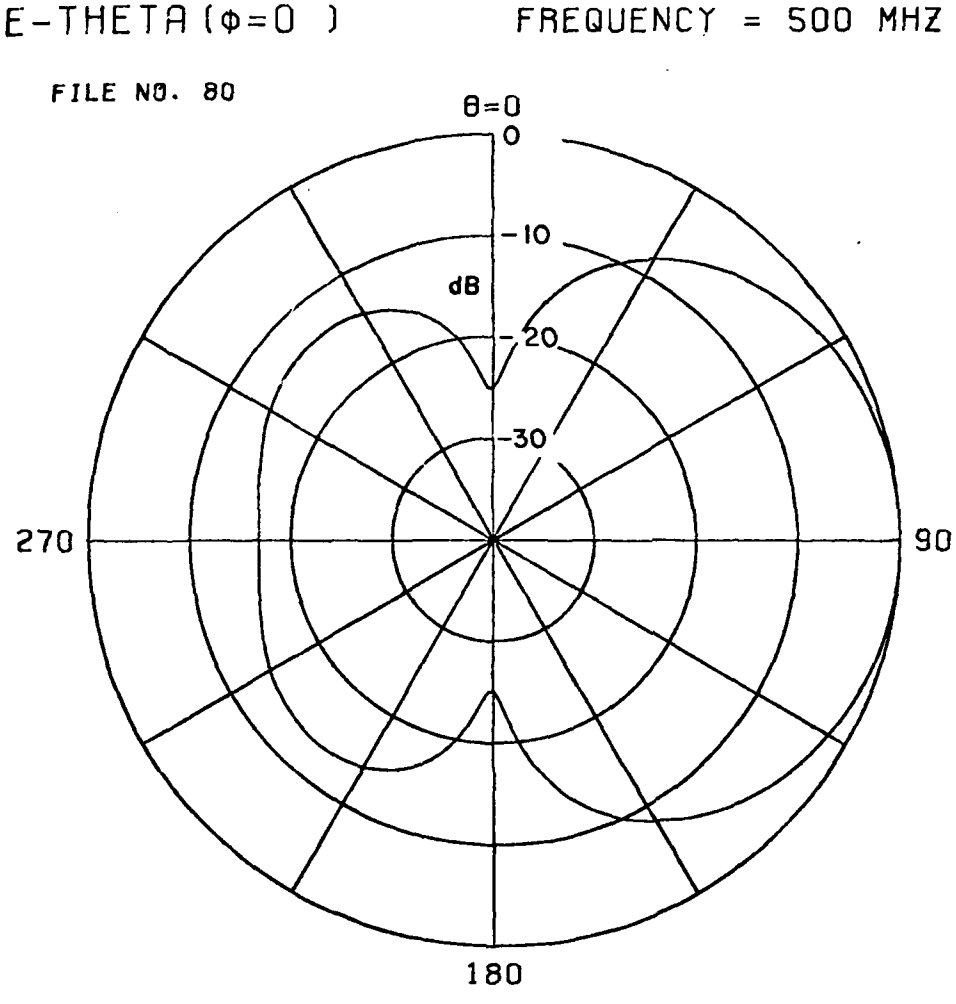

Fig. 2-3(b). Theta component of the far electric field pattern in the vertical plane for the axial dipole of Fig. 2-1 located on the finite length cylinder.

CHAPTER III

RADIATING ELEMENTS ON CIRCULAR CYLINDERS OF INFINITE LENGTH

A. Introduction

The previous chapter presented a method of solving electromagnetic radiation problems by wire-grid modeling of the radiating structure. For practical reasons, this method is limited to structures which are not electrically large. The structure is modeled with wire segments no longer than $\lambda/4$ and surfaces with grids not greater than about $.2\lambda$ by $.2\lambda$. The number of segments and grids determines the number of modes and, correspondingly, the size of the impedance matrix and number of simultaneous equations to solve. The computer storage and running time are approximately proportional to the third power of the number of equations. Electrically large structures require numerous modes for accurate modeling. Thus computer storage limitations and running time expense will limit the size of the structure which may be analyzed by this method. This constraint provides the motivation for considering radiating elements on infinitely long, perfectly-conducting circular cylinders for which a modal solution exists. The modal solution, when combined with data obtained by the method of Chapter II for the current distribution on the radiating element itself, provides an accurate and computationally efficient means for calculating far-field patterns of radiating elements on an electrically long cylinder.

The motivation for requiring a method to examine the patterns of small antennas on long cylinders will become apparent in the next chapter. However, generally speaking, the length of the cylinder does have an effect on the elevation plane pattern and this effect will have significance in Chapter IV.

B. Modal Solutions for Infinite Circular Cylinders

The modal solutions for the total field at any point in space for a plane-wave incident on a perfectly-conducting infinitely long circular cylinder are presented in reference [4] by Burnside. The approach is similar to that of Sinclair [5]; however, it is based on the cylindrically separable fields presented by Richmond [6]. The solutions are divided into two orthogonal polarizations, theta and

phi. Figure 3-1 illustrates the orientation of the coordinate system, antenna elements and polarizations of the incident planewaves. The phi components of the incident fields in the x-z plane, that is for $\phi_i = 0$, are

$$\underline{E}^i_\phi = \hat{\rho}\, e^{jk(z \cos\theta_i + \chi \sin\theta_i)} \tag{3-1}$$

$$\underline{H}^i_\phi = \hat{\theta}\, \frac{e}{Z_o}^{jk(z \cos\theta_i + \chi \sin\theta_i)} \tag{3-2}$$

Z_o is the free space impedance and $k = 2\pi/\lambda$.

The z-component of the incident H-field can be written as

$$H^i_{\phi z} = -\frac{\sin\theta_i}{Z_o}\, e^{jkz \cos\theta_i}\, e^{jkx \sin\theta_i} \tag{3-3}$$

where the Bessel function representation

$$e^{jkx \sin\theta_i} = \sum_{n=-\infty}^{\infty} j^n J_n (k\rho \sin\theta_i)\, e^{-jn\phi} \tag{3-4}$$

may be used to give

$$H^i_{\phi z} = -\frac{\sin\theta_i}{Z_o}\, e^{jkz \cos\theta_i} \sum_{n=-\infty}^{\infty} j^n J_n(k\rho \sin\theta_i)\, e^{-jn\phi} \,. \tag{3-5}$$

Using cylindrically separable fields from Table 3-1, the phi component of the phi polarized incident electric field is

$$E^i_{\phi\phi} = -j\, e^{jkz \cos\theta_i} \sum_{n=-\infty}^{\infty} j^n J'_n (k\rho \sin\theta_i)\, e^{-jn\phi} \tag{3-6}$$

The form of the scattered field can be written

$$E^s_{\phi\phi} = j\, e^{jkz \cos\theta_i} \sum_{n=-\infty}^{\infty} a_n H'^{(2)}_n (k\rho \sin\theta_i)\, e^{-jn\phi}. \tag{3-7}$$

where the a_n's are unknowns which may be evaluated with the appropriate boundary condition. On the surface of the perfectly-conducting cylinder the tangential components of the total E-field must vanish. That is,

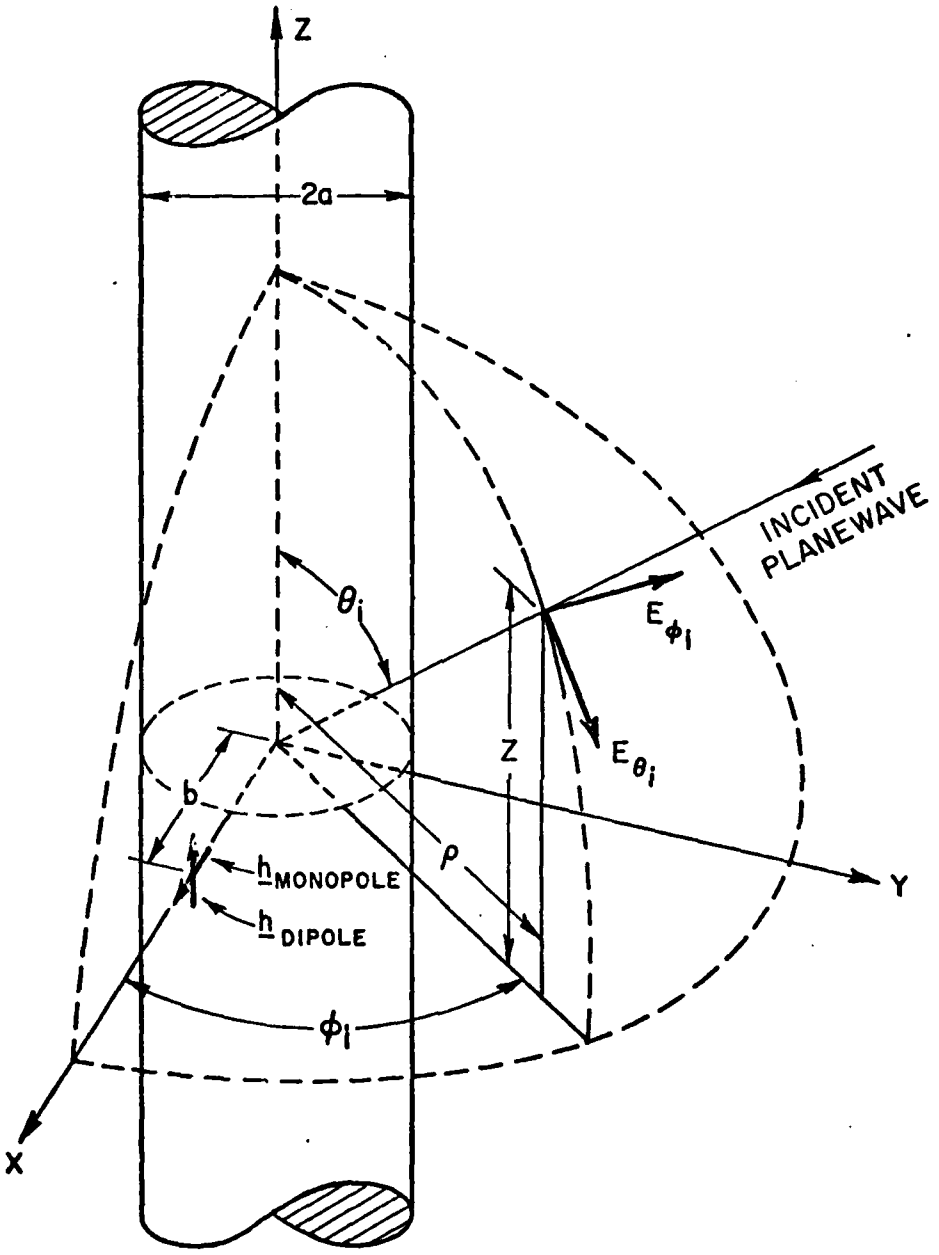

Fig. 3-1. Infinite length circular cylinder with location and orientations of the infinitesimal radial monopole and axial dipole.

TABLE 3-1

TE AND TM FIELDS SEPARABLE IN THE CYLINDRICAL COORDINATE SYSTEM

The harmonic electromagnetic fields listed below satisfy Maxwell's equations in a homogeneous source-free region.

TE Fields			TM Fields		
E_ρ =	$-(j\omega\mu/\rho)$	R P' Z	E_ρ =		R' P Z'
E_ϕ =	$j\omega\mu$	R' P Z	E_ϕ =	$(1/\rho)$	R P' Z'
E_z =	0		E_z =	β^2	R P Z
H_ρ =		R' P Z'	H_ρ =	$(j\omega\varepsilon/\rho)$	R P' Z
H_ϕ =	$(1/\rho)$	R P' Z'	H_ϕ =	$-j\omega\varepsilon$	R' P Z
H_z =	β^2	R P Z	H_z =	0	

The time dependence $e^{j\omega t}$ is understood. R is a function of ρ only, P is a function of ϕ only, and Z is a function of z only. Primes indicate differentiation with respect to ρ, ϕ or z. The functions satisfy the following differential equations:

$$\rho \frac{d(\rho R')}{d\rho} + (\beta^2 \rho^2 - m^2) R = 0$$

$$P'' = -m^2 P$$

$$Z'' = -h^2 Z$$

where

$\beta^2 + h^2 = \omega^2\mu\varepsilon$, and β and h are constants.

Some solutions of these differential equations are listed below.

$R(\rho)$ =	$P(\phi)$ =	$Z(z)$ =
$J_m(\beta\rho)$	$\cos m\phi$	$\cos hz$
$N_m(\beta\rho)$	$\sin m\phi$	$\sin hz$
$H_m^{(1)}(\beta\rho)$	$e^{jm\phi}$	e^{jhz}
$H_m^{(2)}(\beta\rho)$	$e^{-jm\phi}$	e^{-jhz}

$$E_{\substack{\\ tan}} = 0 = E^{i}_{\phi\phi}\ (\rho = a) + E^{s}_{\phi\phi}\ (\rho = a) \quad . \tag{3-8}$$

Substituting Eq. (3-6) and (3-7) into Eq. (3-8), and solving for a_n, gives

$$a_n = j^n \frac{J_n'\ (ka \sin \theta_i)}{H_n^{(2)\prime}(ka \sin \theta_i)} \quad . \tag{3-9}$$

The total field at any observation point is now specified by the above relations in conjunction with Table 3-1. Of particular interest to problems solved in this investigation are the following:

$$E_{\phi\rho} = \frac{e^{jkz \cos \theta_i}}{k\rho \sin \theta_i} \sum_{n=1}^{\infty} 2n\, j^{n+1} \left[J_n(k\rho \sin \theta_i) - \frac{J_n'\ (ka \sin \theta_i)}{H_n'^{(2)}\ (ka \sin \theta_i)} H_n^{(2)}\ (k\rho \sin \theta_i) \right] \sin n(\phi - \phi_i) \tag{3-10}$$

$$E_{\phi z} = 0 \quad . \tag{3-11}$$

For theta polarized incident plane waves:

$$E_{\theta\rho} = -j \cos \theta_i\, e^{jkz \cos \theta_i} \sum_{n=0}^{\infty} \varepsilon_n\, j^n \left[J_n'\ (k\rho \sin \theta_i) - \frac{J_n(ka \sin \theta_i)}{H_n^{(2)}\ (ka \sin \theta_i)} H_n'^{(2)}\ (k\rho \sin \theta_i) \right] \cos n(\phi - \phi_i) \tag{3-12}$$

$$E_{\theta z} = -\sin \theta_i\, e^{jkz \cos \theta_i} \sum_{n=0}^{\infty} \varepsilon_n\, j^n \left[J_n\ (k\rho \sin \theta_i) - \frac{J_n(ka \sin \theta_i)}{H_n^{(2)}\ (ka \sin \theta_i)} H_n^{(2)}\ (k\rho \sin \theta_i) \right] \cos n(\phi - \phi_i) \tag{3-13}$$

where $$\varepsilon_n = \begin{cases} 1, & n = 0 \\ 2, & \text{otherwise} \end{cases} \quad . \tag{3-14}$$

These components of the electric field will be the ones needed to calculate the far fields radiated by infinitesimal radial monopoles and axial dipoles located near the infinite cylinder. The antennas are very short in terms of wavelengths so that the open circuit voltages they receive will cause negligible distortion to the field which would exist in their absence. The open circuit voltages are equal to the product of the effective heights of the radiators times the component of electric field intensity parallel to their axes. That is,

$$\underline{h}_{\text{monopole}} = \ell[\hat{\theta}\, E_{\theta\rho}\ (\rho = b) + \hat{\phi}\, E_{\phi\rho}\ (\rho = b)] \tag{3-15}$$

and

$$\underline{h}_{\text{dipole}} = \ell[\hat{\theta}\, E_{\theta z}\ (\rho = b) + \hat{\phi}\, E_{\phi z}\ (\rho = b)] \tag{3-16}$$

where ℓ is the effective length of the monopole or dipole without the cylinder present. Here the antennas are located at $\phi = 0$, $z = 0$ and the phase is referred to the center of the cylinder.

For the case when the antenna elements are transmitting, the electric field is given by

$$\underline{E}\ (r,\theta_i,\phi_i) = \frac{j\, Z_o\, I\, e^{-jkr}}{2\,\lambda r}\ \underline{h}\ (\theta_i,\phi_i) \tag{3-17}$$

where I is a complex current excitation. The next section shows how these equations may be used to find the far field of larger radiators of different shapes.

C. A Hybrid Method

The expressions for the distant fields radiated, given in the previous section, are based on infinitesimal elements of electric current. To determine the far fields of an arbitrary antenna radiator in the presence of the infinite cylinder, integration over the equivalent aperture currents must be performed. This can be done numerically by superposition of the fields from the infinitesimal currents weighted by the appropriate complex current coefficient. That is,

$$\underline{E}_{\text{total}}(r,\theta_i,\phi_i) \cong \frac{j\, Z_o\, e^{-jkr}}{2\,\lambda r} \sum_{n=1}^{N} I_n\, \underline{h}_n\ (\theta_i,\phi_i - \phi_n,\ z_n) \tag{3-18}$$

where I_n is the current of the n^{th} element which has the appropriate effective height $\underline{h}_n$ and whose position is located by ϕ_n, Z_n.

In order to find the I_n's necessary for this calculation, the methods of Chapter II may be employed. Chapter II describes how a discrete current distribution on an antenna element located on a finite cylinder is calculated using wire-grid modeling. The assumption that the currents induced on the antenna elements for a particular excitation will be almost identical for finite and infinite cylinder cases is made. This is especially true for cases where the radiating elements are resistively loaded as those which are investigated in Chapter IV. So, the current distribution calculated by the methods of Chapter II can be used to find the complex weighting coefficients I_n, of Eq. (3-18).

This technique is called a hybrid method since it combines the thin wire methods of the previous chapter with the modal solution of this chapter. Thus, the arbitrary radiator is divided into segments oriented as radial monopoles or axial dipoles and of extent no greater than .1λ. Currents at the endpoints are found using the thin-wire computer program. The complex current coefficient for any given segment would be the average of its endpoint currents multiplied by its length in wavelengths normalized by a normalizing factor. The far field will be the sum of all the fields radiated by each segment.

D. Application of the Hybrid Method

The hybrid method discussed in the previous section provides an efficient means for calculating the far-field patterns of radiators located on or near an infinite cylinder. At the end of Chapter II, the results of the sinusoidal reaction technique applied to a radial monopole and axial dipole on a finite cyliner were presented. The finite length of the cylinder has very pronounced effects on the far-field patterns. Computer capability makes extending the cylinder length by wire-grid modeling impractical. Figure 2-1 shows the cylinder length that was modeled to be 35 cm which is only 0.875λ at 750 MHz. To find the patterns of radiators on longer cylinders, the modal solution of this chapter could be applied. The infinite cylinder will be a good approximation to finite cylinders of a few wavelengths since the radiators considered are electrically quite small.

As a comparison of methods, to show the effects of the finite cylinder, and to provide a reference for subsequent discussions, the radiators of Fig. 2-1 are analyzed on an infinite cylinder. The equations of the far-field expressions are programmed along with the means for computing the complex weighting factors using the currents calculated for the radiators in Chapter II.

Figures 3-2 and 3-3 show the far-field patterns decomposed into phi and theta polarizations in the two principal planes of the radial

monopole and the axial dipole, respectively. Comparing these results with those on a finite cylinder, Figs. 2-2 and 2-3 give the following insights. Phi components of electric field radiated by the radial monopole are not affected by the shortness of the cylinder. Theta components of the field lose their symmetry and front-to-back ratio in the elevation plane. The axial dipole transmits no phi component for either cylinder. The theta components are not greatly different at the frequency shown.

In the following chapter, the method of this chapter along with the method of Chapter II will be applied to investigate a new direction finding scheme.

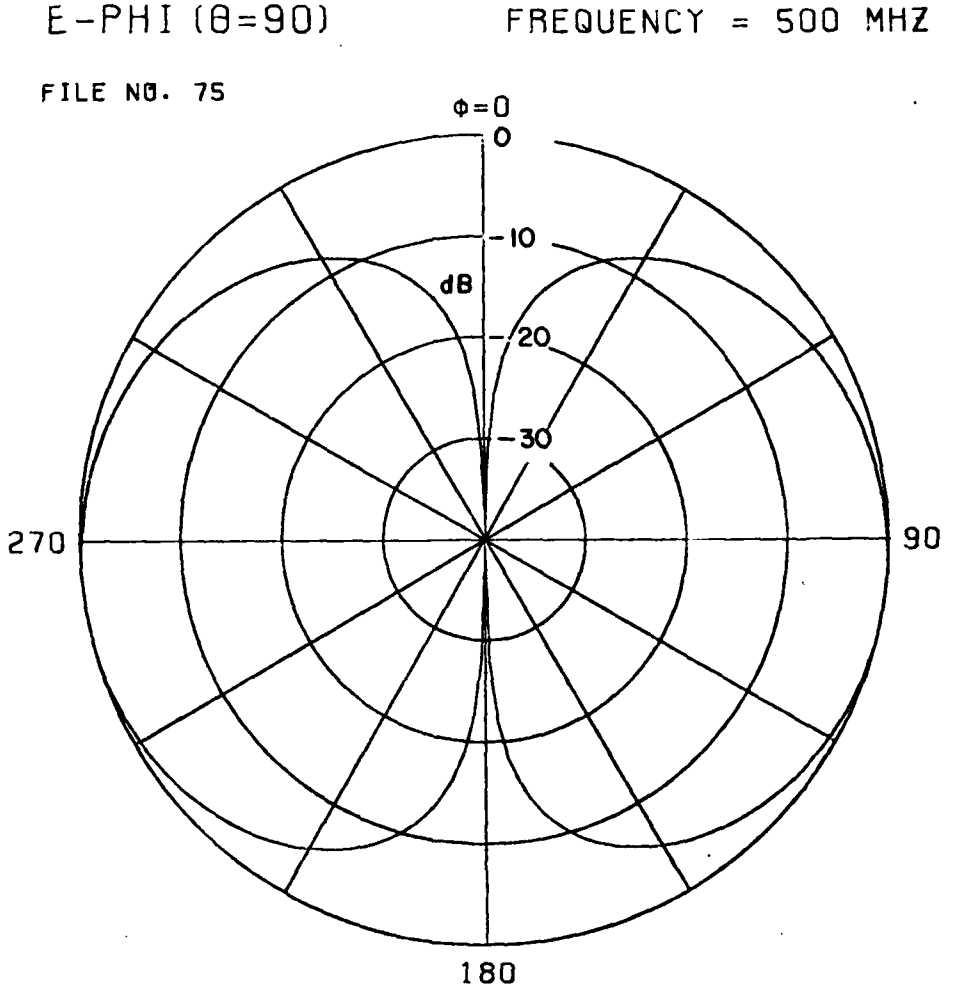

Fig. 3-2(a). Phi component of the far electric field pattern in the horizontal plane for the radial monopole of Fig. 2-1 located on the infinite length cylinder.

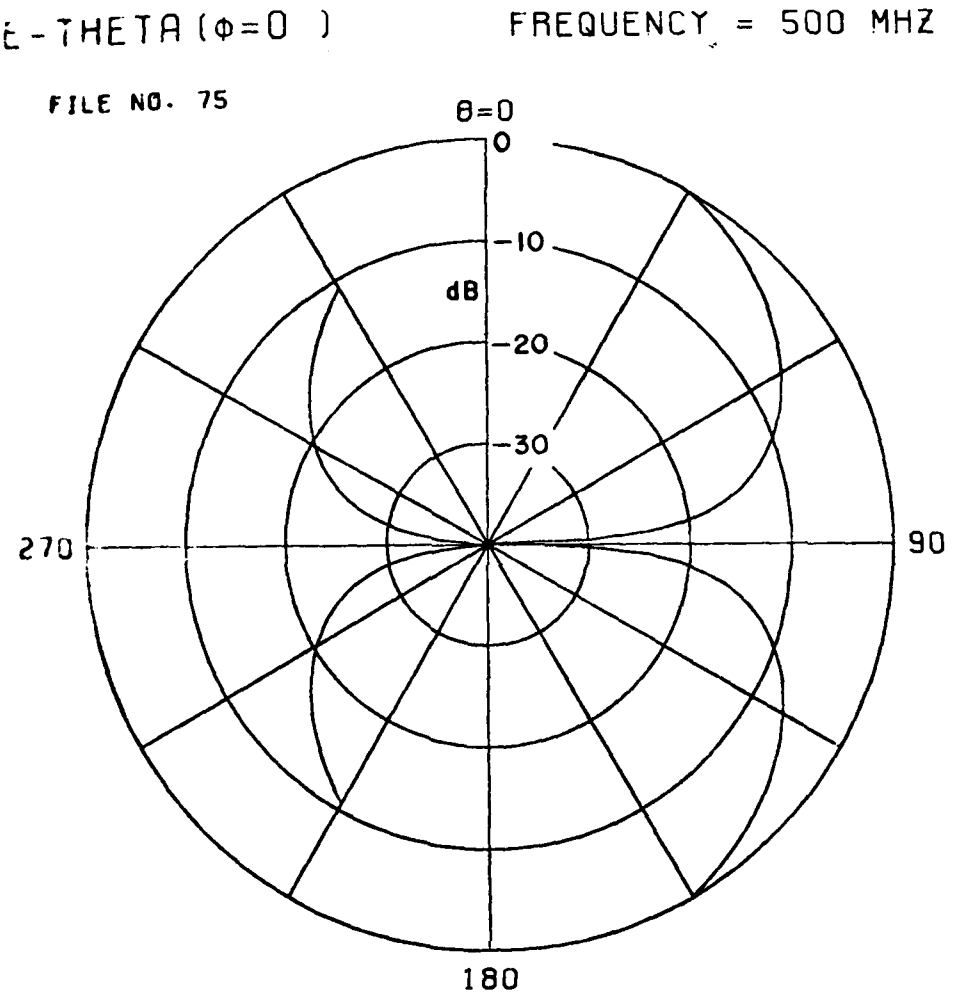

Fig. 3-2(b). Theta component of the far electric field pattern in the vertical plane for the radial monopole of Fig. 2-1 located on the infinite length cylinder.

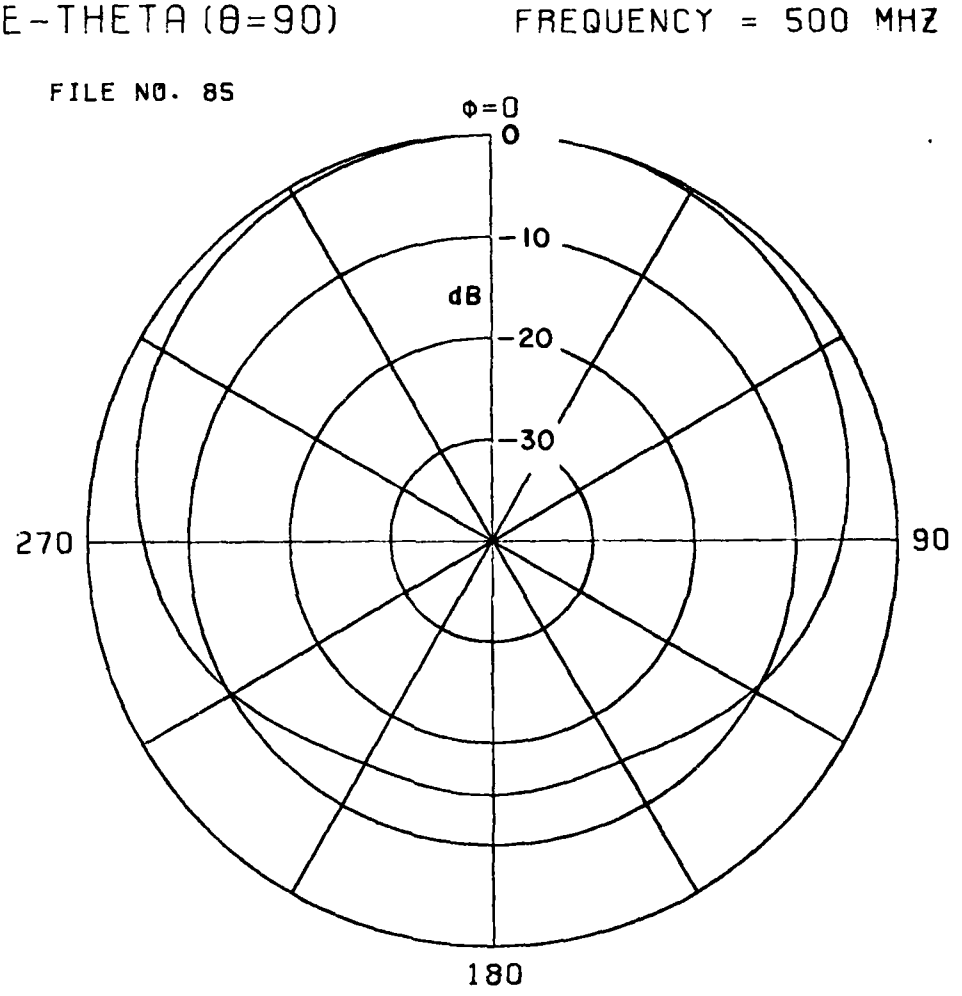

Fig. 3-3(a). Theta component of the far electric field pattern in the horizontal plane for the axial dipole of Fig. 2-1 located on the infinite length cylinder.

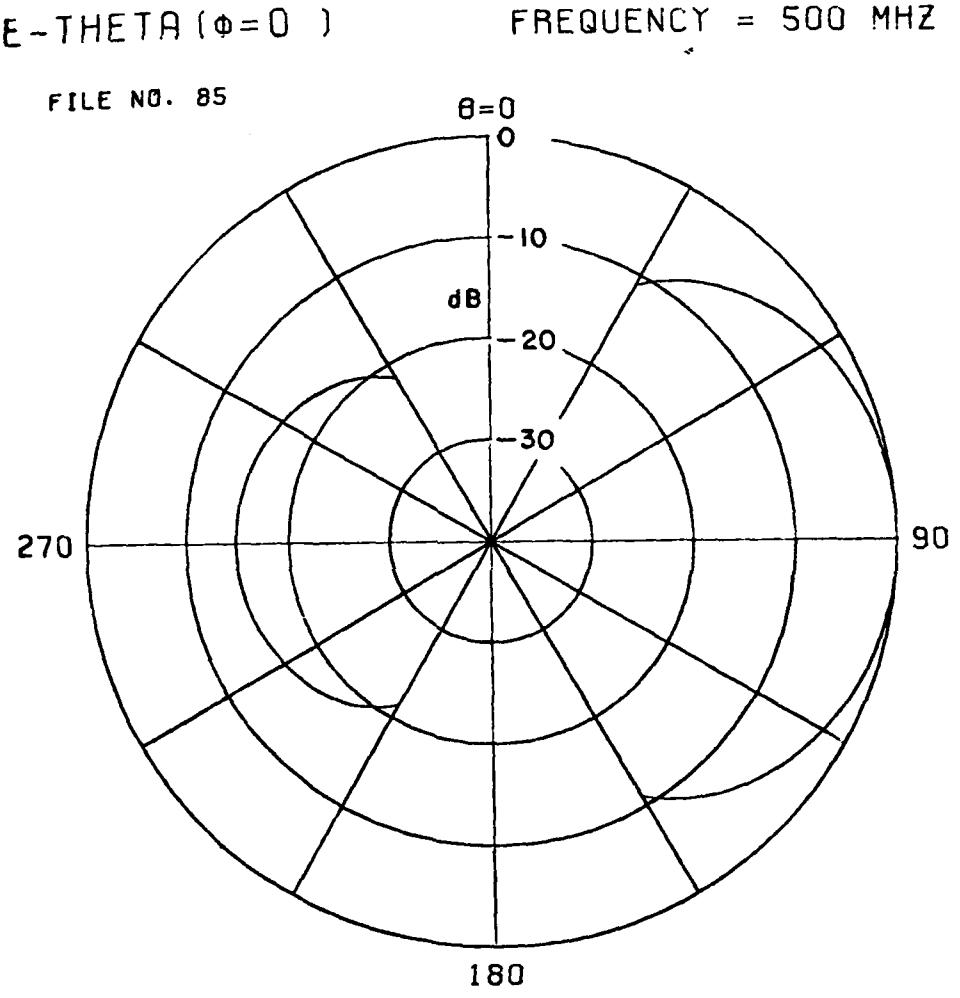

Fig. 3-3(b). Theta component of the far electric field pattern in the vertical plane for the axial dipole of Fig. 2-1 located on the infinite length cylinder.

CHAPTER IV

PROPOSED DIRECTION FINDING SYSTEM

A. Introduction

One objective common to all radar and direction finding (DF) systems is the determination of where the target is relative to the system location. One parameter basic to this determination is the azimuthal angle in the system's reference coordinate system. This chapter discusses a DF system proposed to work under the constraints enumerated in Chapter I. A system which works over a frequency range is demonstrated and its limitations discussed. The particular antenna configuration which is used to demonstrate the system is one of several which were investigated and is not an optimal design for a particular DF system. It was chosen simply as a vehicle to present the concept of the proposed DF system.

B. Method of Angle-of-Arrival Determination

Many methods of angle-of-arrival determination are used in radar and DF systems. The methods depend on available information about the incident or return signal and the capability of the receiving system, including the antenna, to process this information. Many systems use highly directional antennas which electrically or mechanically scan the area of interest. This study is restricted to electrically small antennas which are stationary and necessarily have broad patterns of low directivity. Many systems use frequency and phase information analyzed by a complex processor to determine angle of arrival. This study proposes a system requiring only the most elementary processing which does not need to know the frequency or phase of the incident signal within a broad frequency band. Many systems receive only certain polarizations of incoming signals, while the proposed system responds to any arbitrarily polarized signal.

The patterns of electrically small radiators in the presence of an electrically larger cylinder are restricted to several basic shapes. This result is because any practical element less than a quarter wavelength in extent has the same pattern shape independent of its current distribution. In the azimuthal plane, two basic shapes result for the two orthogonal polarizations; theta (vertical) polarization and phi (horizontal) polarization. These transmitting

patterns will, by reciprocity, result in received or induced voltage patterns of the same shape. The two basic received voltage patterns are shown in Fig. 4-1. Section E of this chapter demonstrates by a specific example that these patterns can be received over a broad frequency band. Section E also demonstrates that an arbitrarily polarized incoming signal can be decomposed into these two patterns.

In general, determination of angle of arrival using received voltage patterns, such as in Fig. 4-1, could be accomplished as follows: Space three receiving ports, one every 120°, about the cylinder. Consider first the theta polarized component of the received voltage pattern, V-theta (ϕ). This pattern has one simple maximum and is symmetric about phi equal 180° line. Three such patterns spaced 120° apart would allow unambiguous angle-of-arrival determination by simple port voltage comparison processing. These three patterns are illustrated in Fig. 4-2(a). Figure 4-2(b) shows how the 360° of azimuth angle can be divided into six sections by comparison of voltage magnitude levels. This figure also shows that the ratio or the difference of largest to next largest port voltage gives a unique number for each azimuth angle in its range. This algorithm would be quite simple to implement. It is not presented as the best or optimal scheme, but merely to demonstrate that the angle of arrival may be uniquely determined from purely theta polarized voltages induced on the three ports.

The same method can be applied to the port voltages induced by purely phi polarized incident signals, V-phi (ϕ), such as shown in Fig. 4-1. This pattern has two simple maxima and is symmetric about phi equal 90° or 180° line, that is, the pattern repeats every 180° instead of every 360°. Dividing the azimuthal plane by comparison of voltage magnitude levels gives six pairs of sections. The number obtained by forming the ratio or difference will be the same for two angles 180° apart. The angle of arrival obtained from the purely phi polarized induced port voltages is either correct or else wrong by 180°. This may not be a serious ambiguity for the following reasons: In practical systems the direction finding signal will rarely be purely theta or phi polarized, but will contain components of both. Which of the two angles obtained from the phi scheme is correct can be determined by the angle given by the theta scheme. For the frequency ranges considered in this study, theta components of the incoming signals will be dominant because of the propagation properties of practical media.

Angle of arrival can be unambiguously determined if port voltage patterns illustrated in Fig. 4-1 can be obtained. If they are received over a frequency band, this method determines the angle of arrival of an incident signal using small passive antenna elements without knowing the frequency, phase or polarization of the incoming signal.

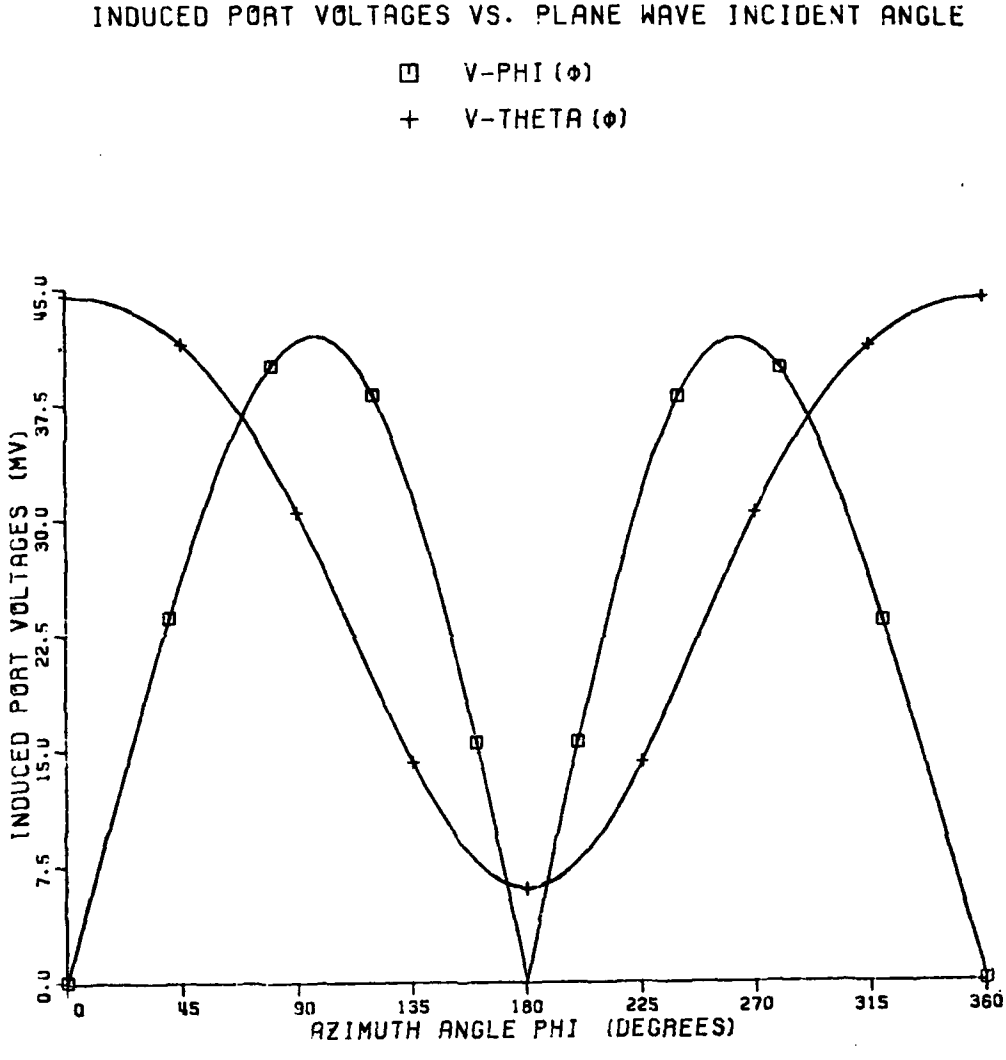

Fig. 4-1. Phi and theta components of a basic received voltage pattern.

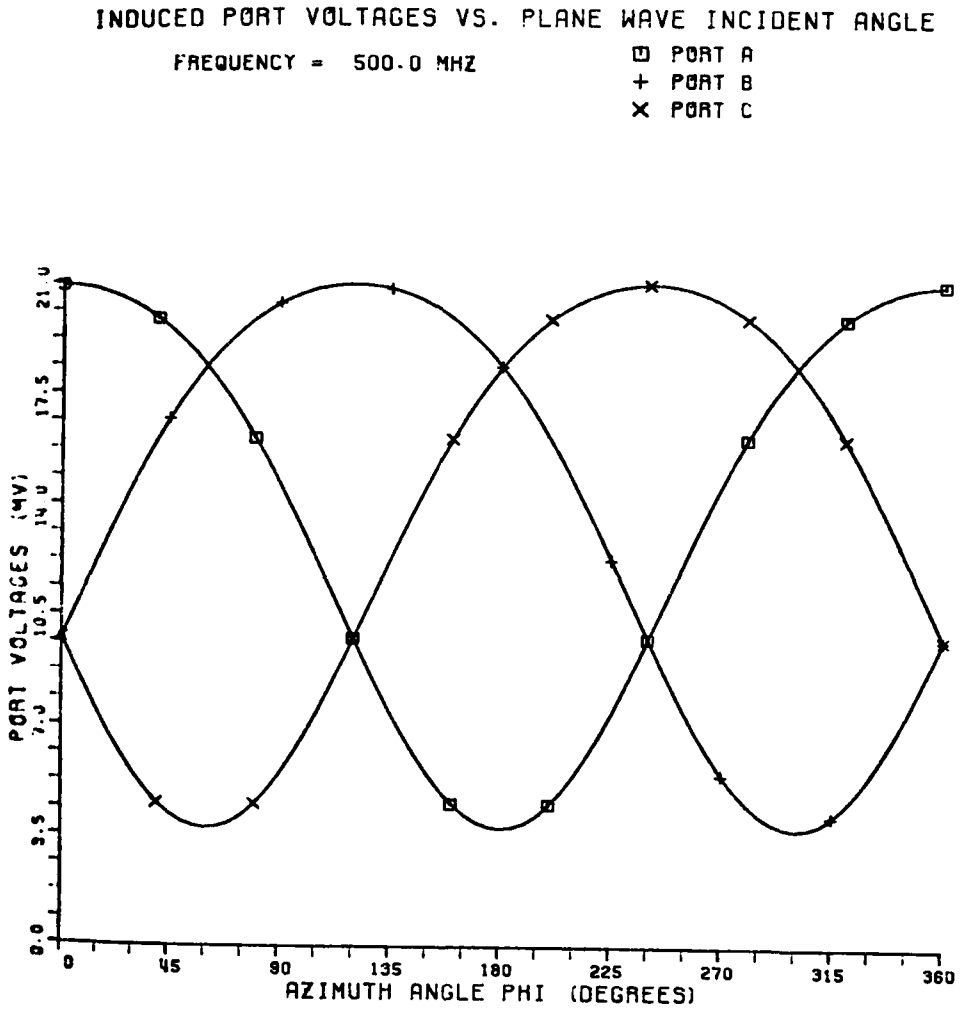

Fig. 4-2(a). Theta component of the received voltage pattern for three input ports spaced 120° apart around the cylinder.

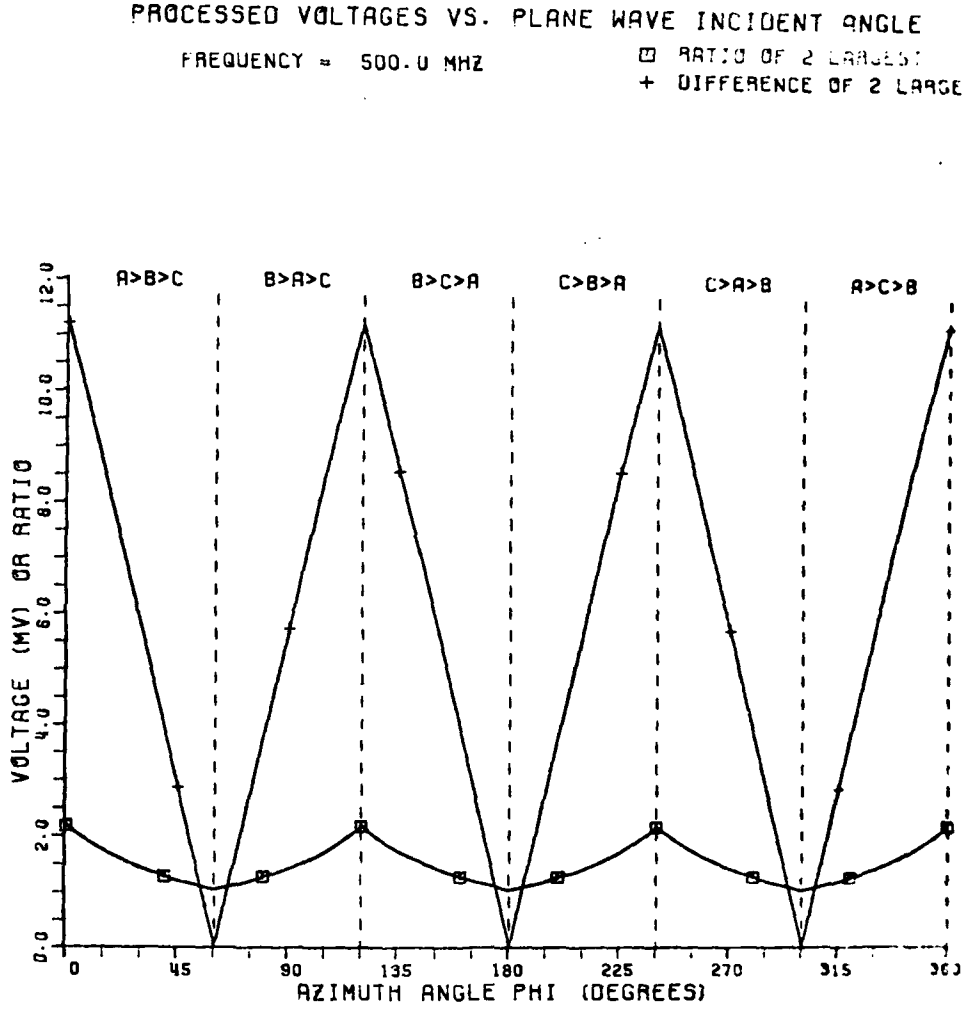

Fig. 4-2(b). Determination of angle of arrival by simple comparison of received port voltages of Fig. 4-2(a).

C. Problems With Simple Radiators

The previous section demonstrated the desirability of obtaining patterns like those shown in Fig. 4-1 over as broad a frequency band as possible. For a purely theta polarized incident signal, any antenna element close to a large conducting cylinder that has a vertical arm less than a quarter wavelength in extent (or dipole-type feed less than half wavelength) will have a horizontal plane pattern similar to V-theta (ϕ) of Fig. 4-1. Similarly, for a purely phi polarized incident signal, any antenna element close to a large cylinder that has a horizontal arm less than a quarter wavelength in extent will have a horizontal plane pattern similar to V-phi (ϕ) of Fig. 4-1. This was demonstrated clearly for various radiators analyzed by the method of Chapter II.

These facts could also be argued as follows: Any arbitrarily shaped antenna in the presence of the cylinder can be decomposed by the principle of superposition into radiators with only vertical or horizontal components. These two basic elements have pattern shapes that were illustrated in Chapters II and III, Figs. 2-2, 2-3, 3-2, and 3-3. These patterns are transmitting far-field patterns, but by reciprocity the receiving port voltage plots can be predicted. The theta component of the vertical dipole field pattern in the horizontal plane, Fig. 2-3(a), would have the same receiving pattern as V-theta (ϕ) of Fig. 4-1. Similarly, the phi component of the radial monopole field pattern, Fig. 2-2(a) would have the same receiving pattern as V-phi (ϕ) of Fig. 4-1.

Superposition of these basic elements and their corresponding field patterns could be used to model any arbitrary vertical and/or horizontal radiating element with the resulting horizontal plane patterns being similar to V-theta (ϕ) and V-phi (ϕ) of Fig. 4-1. So for purely phi or theta polarized incident signals, many acceptable antenna elements exist which give the desired patterns of Fig. 4-1.

Consider a radiating element which has both horizontal and vertical arms (bent monopole, half-loop, etc.). If the incoming signal is purely theta or phi polarized, then by applying the appropriate angle of arrival determination method, this type of element spaced every 120° would suffice for the DF system. If, however, the polarization of the incident signal is unknown or not pure, that is, arbitrary, then the scheme breaks down. With unknown polarization, which scheme should be applied, theta or phi, cannot be determined. For any given incoming signal, the two schemes or algorithms give different answers for the angle of arrival. If the polarization is arbitrary, somewhere between purely theta or phi, this problem is complicated because neither scheme would give the correct answer since the received voltage pattern would be some weighted combination of the V-theta (ϕ) and V-phi (ϕ) of Fig. 4-1. This combined pattern would be different for each unique polarization between purely phi or theta.

A solution to this problem could be achieved if the incoming signal could be separated into its phi and theta components. Ideally, two elements might be used to cover all possible polarizations if one responded only to theta polarized signals and the other to only phi polarization. The theta sensitive element would use the scheme described by Fig. 4-2. The phi sensitive element would use a similar but shifted algorithm to give the angle of arrival, or the angle +180°, as described in Section B.

The axial or vertical dipole of Chapter II, Fig. 2-1, offers the desired theta sensitive element with negligible phi sensitivity. A search for a radiator in the presence of the cylinder which is sensitive to only phi polarized incident signals from all angles poses a difficult problem. Any element containing horizontal arms near the cylinder produces theta components of the far zone electric field which for some elevation angles are as strong as the phi components. This was investigated for various radiators, including radial monopoles, circumferential dipoles, circumferential slots, and loops. So, in the presence of the cylinder, two elements which are sensitive to the two major polarizations independently are unavailable.

The next section demonstrates that the proper combination of two elements facilitates the cancellation of components of one polarization.

D. A Method for Separating Polarizations

To achieve the desired patterns of Fig. 4-1 over a frequency band, and thus form a DF system, the incoming signal must be decomposed into the two orthogonal polarizations. For the reasons indicated in the previous section, this is not possible using radiating elements which are independently sensitive to the two polarizations. However, two symmetric elements correctly positioned and properly combined do provide the desired mechanism for separating the polarizations.

Consider a pair of vertically oriented radiators such as half-loops mounted on the cylinder as illustrated in Fig. 4-3. One of the pair is mounted with the input port at the bottom, the current being driven to the top. The other is mounted as closely as possible to the first element but inverted so that it is fed at the top and terminated at the bottom. Careful study of the field patterns or induced port voltage patterns shows that the two elements have the same phi component patterns which are in phase. Theta component patterns are also the same, at least in the azimuthal plane, but are 180° out of phase. Examination of the element orientations and physical insight justifies these results. The pair of elements has vertical components, producing theta fields, which are driven in opposite directions, 180° out of phase. The pair of elements has radial components, producing phi fields, which are driven in the same direction and are therefore in phase. The radial components are

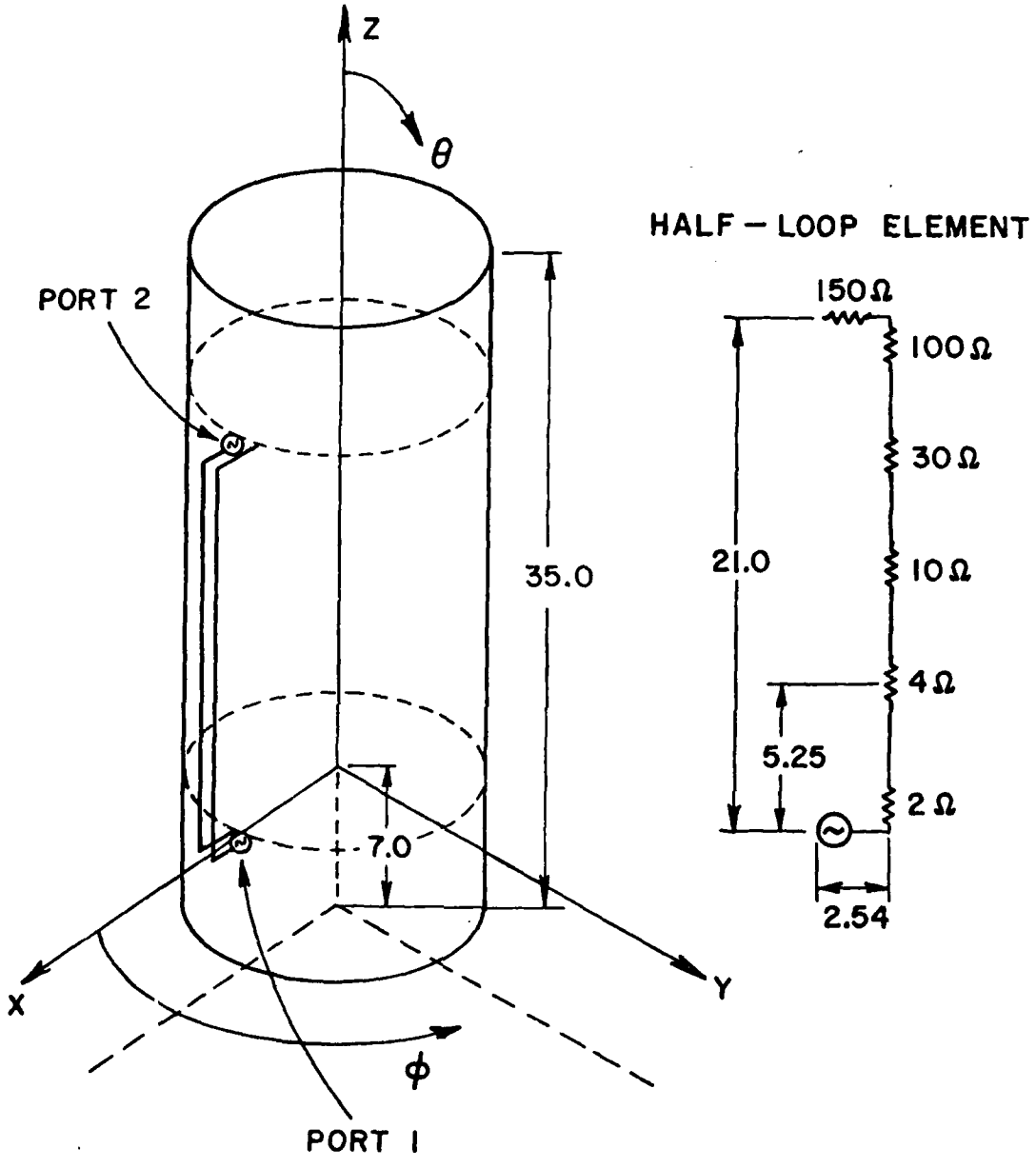

Fig. 4-3. Two resistively loaded half-loop radiating elements symmetrically located on the finite cylinder. The dimensions are in centimeters and the coordinate systems are the ones used in the patterns which follow.

displaced from each other in the z direction, but this does not greatly affect their phases, since phi components are independent of z.

If the ports of these pairs of elements are considered as input terminals, then incoming signals will induce port voltages which can be combined to separate the two polarizations. Adding the two port voltages will result in cancellation of the theta components of the incoming signal since they are equal but 180° out of phase on the two ports. The in-phase and equal phi components will add, giving twice what appears on each port. Similarly, subtracting the two port voltages will cancel the phi contributions and double the theta component of one port taken alone. For this method to be effective, the elements must be symmetric so that their pattern magnitudes are equal. They must be placed as close together as is practical so that their phase centers are as nearly superimposed as possible over the frequency range. It is important that the ports maintain their relative phase difference over the frequency range and for all aspect angles.

The next section will demonstrate how this method works for some pairs of radiating elements. By decomposing the incoming signal into its two basic polarizations, it becomes possible to determine the angle of arrival. The process would involve two steps. First, adding the two port voltages of the three pairs of elements spaced around the cylinder would give only the phi components of the incoming signal. These three voltage levels would be compared as discussed in Section B to give the angle of arrival. Second, subtracting the two voltages of three pairs of elements leaves only theta components of the incoming signal. These would be compared to give the angle of arrival. By this method, the desired voltage patterns of Fig. 4-1 can be achieved, and thus the angle of arrival can be determined for a signal of unknown frequency and arbitrary polarization.

E. Results of the Method Applied to Half-Loops

Figure 4-3 shows a pair of half-loops attached to a cylinder. This type of antenna element was one of several studied in the presence of an electrically larger conducting cylinder and was chosen to demonstrate the method of separation of polarization discussed in the previous section. The half-loops are resistively loaded to achieve desired input impedance characteristics as discussed in the next section. The DF system is proposed to work over as large a frequency band as possible. To study this, the physical dimensions of the cylinder and half-loops are held constant and its antenna characteristics are analyzed over a frequency range.

For the fixed dimensions given in Fig. 4-3, the half-loops exhibit desired characteristics over the frequency range 250 MHz to 750 MHz, a three-to-one band. The exact bandwidth would depend

on many system specifications such as minimum antenna efficiency, [illegible] allowable mismatch, signal-to-noise specifications of the incoming signal, desired accuracy of the angle-of-arrival determination, processing capability of the receiver, etc. This study does not make exact specifications of these kinds and only considers general characteristics desirable to all DF systems. The half-loops specified in Fig. 4-3 are not an optimal or final design element for a particular system. They do, however, demonstrate the success of the concept of the DF system discussed in this chapter.

Figure 4-4 shows the received voltages combined as a function of azimuthal angle in the horizontal plane as described in Section D. Three frequencies are included to demonstrate how the patterns behave over a band. The incoming signal is 45° polarized, that is, it contains both phi and theta components. This is accomplished as follows. First, the induced port voltages at Port 1 and Port 2 are calculated by the methods of Chapter II for a theta polarized incident wave of magnitude 1.0 V/m. The induced port voltages for a phi polarized incident wave are then calculated. The complex voltages obtained for the two polarizations are then added at Port 1 and Port 2. The voltages at Port 1, $V_1(\phi)$, and at Port 2, $V_2(\phi)$, are those that would be induced by a 45° polarized incident wave of magnitude $\sqrt{2}$ V/m. The polarizations may now be separated by the method of Section D. Addition of voltages at Port 1 to those at Port 2 gives V-phi (ϕ), and their difference gives V-theta (ϕ).

The above processes can be described by the following equations:

$$V_{\text{phi Port 1}}(\phi) + V_{\text{theta Port 1}}(\phi) = V_1(\phi)$$

$$V_{\text{phi Port 2}}(\phi) + V_{\text{theta Port 2}}(\phi) = V_2(\phi)$$

$$V_{\text{phi}}(\phi) = V_1(\phi) + V_2(\phi)$$

$$V_{\text{theta}}(\phi) = V_1(\phi) - V_2(\phi)$$

Figure 4-4 shows the results of this process for three frequencies in the horizontal plane. The patterns have the same shape as those of the desired patterns which Section B discussed as being capable of angle-of-arrival determination. Note that the theta polarized voltage patterns all have the desired single maximums which occur at the same azimuth angle for the frequency range studied. These patterns are ideally suited to the determination of incidence angle by the method described. The phi polarized patterns are not quite as constant over the frequency range. The maxima occur over a range of 15 degrees of azimuth angle. This reduces the accuracy of the algorithm used to determine the angle of arrival for this polarization by approximately 8 degrees or less. Depending on the specification of a particular system, this may present a problem or be acceptable. So, in the

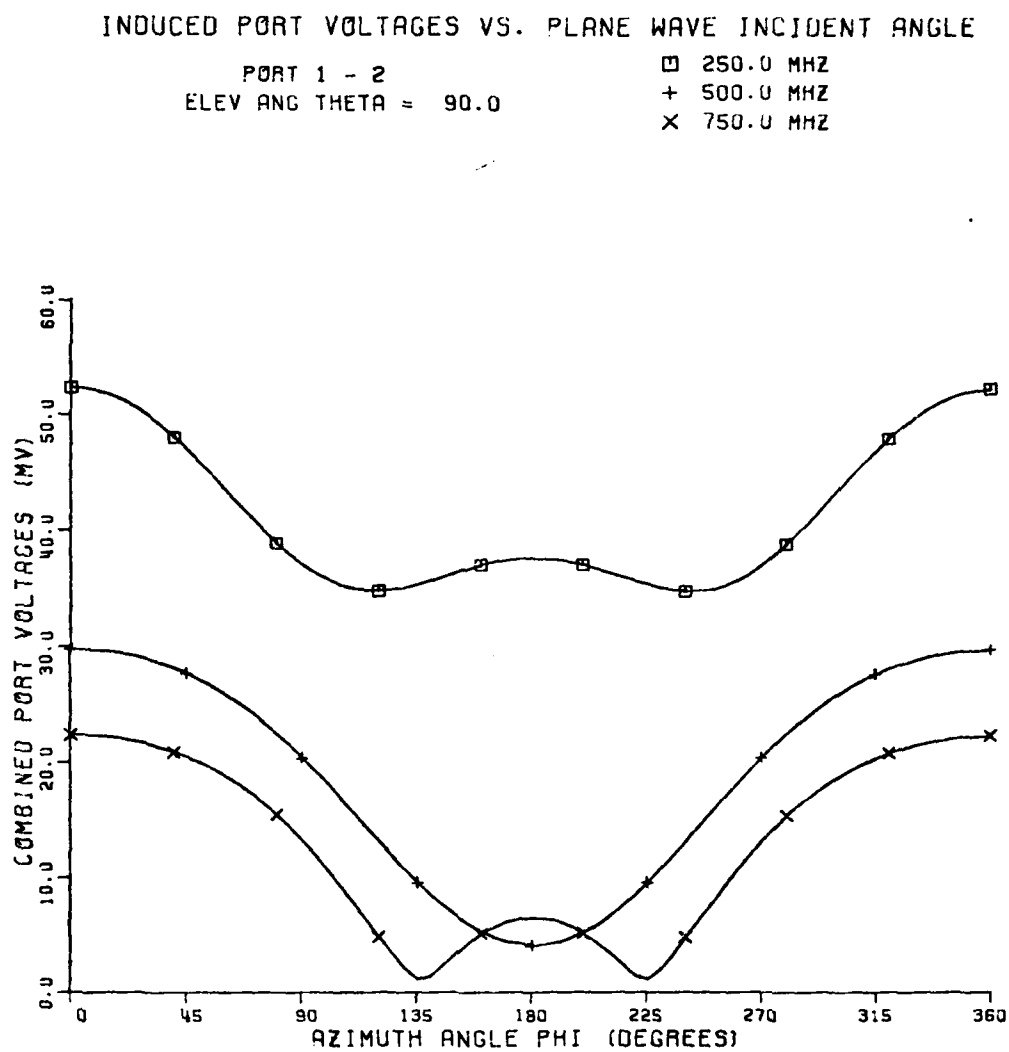

Fig. 4-4(a). Theta component of received voltage pattern obtained by subtracting voltage at Port 1 from Port 2. Three frequencies are shown. The incident wave is in the horizontal plane. The half-loop elements are on the finite cylinder.

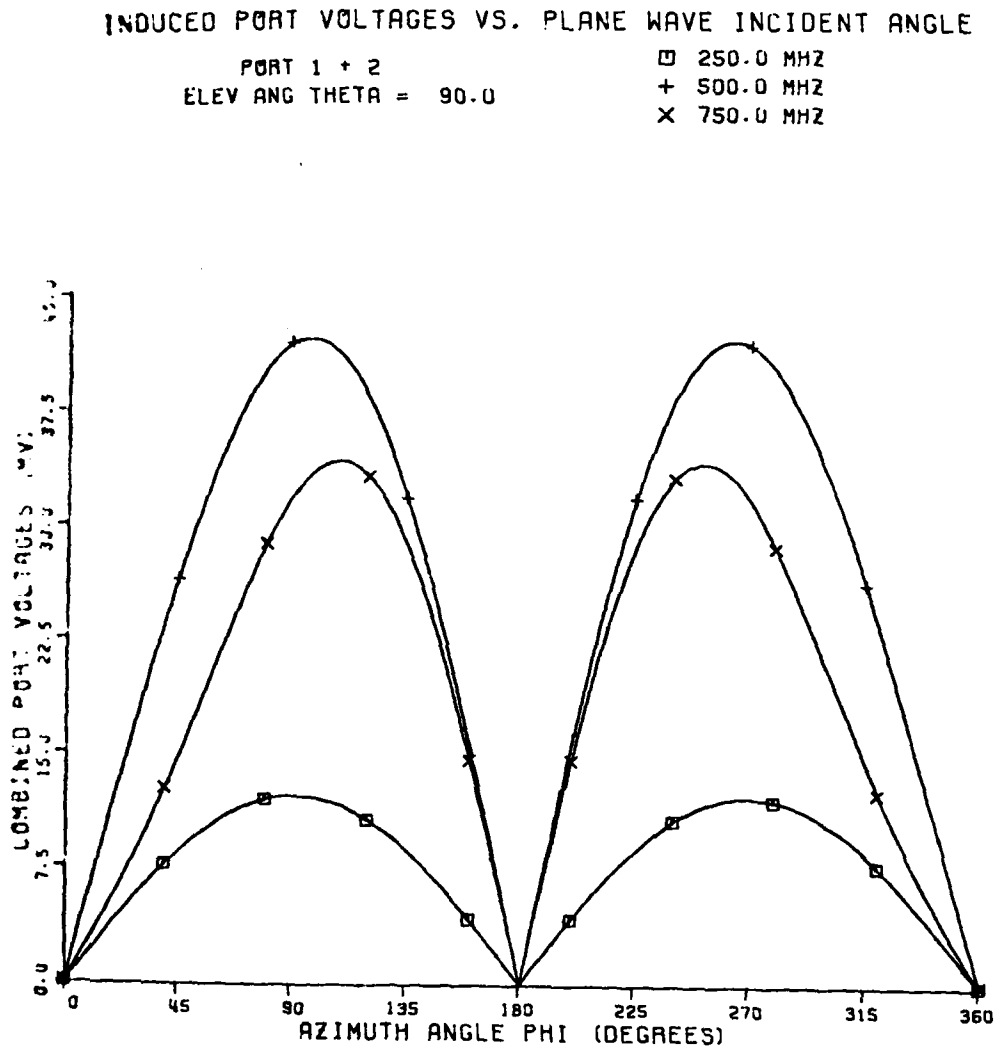

Fig. 4-4(b). Phi component of received voltage pattern obtained by adding voltage at Port 1 and Port 2. Three frequencies are shown. The incident wave is in the horizontal plane. The half-loop elements are on the finite cylinder.

horizontal plane, the method of separation of polarization applied to the pairs of half-loop elements permits angle-of-arrival determination over a three-to-one frequency range for incoming signals of any polarization.

Extension of the concept of separation of polarization for determination of azimuthal angle of arrival for incoming signals from some elevation angle other than the horizon presents some interesting difficulties. Figures 4-5 and 4-6 show what happens when the same method is applied to incoming signals from elevation angles higher than the horizon. Figure 4-5 shows the combined voltage patterns for an incoming signal 10° above the horizon. The patterns have shifted slightly where maxima and minima occur. This would result in a corresponding decrease in the accuracy of determined angle of arrival. Figure 4-6 shows that for an elevation angle of 20°, the patterns have changed and shifted enough that applying the algorithms would result in fairly large errors.

The reason for the problems as elevation angles are increased is due to asymmetries in the elevation plane patterns of the half-loop radiator. This is most clearly demonstrated by looking at the transmitting elevation plane field patterns. Specifically, Fig. 4-7 shows the theta component of the far electric field in the elevation plane for a single half-loop excited from bottom to top. These patterns were calculated using the method of Chapter II, the finite cylinder case. As illustrated, over the frequency range, the patterns are not symmetric about a line for theta equal to 90° representing the horizon. A half-loop excited from top to bottom would have the patterns of Fig. 4-7 but inverted by 180°. The asymmetry about the horizon causes difficulties for elevation angles when applying the method of separation of polarization discussed in Section D. These figures show transmitting patterns but by reciprocity the induced port voltages are proportional, that is, they have the same shape.

Consider, for example, the value of E-theta at 750 MHz for an elevation angle 30° produced by the half-loop excited from bottom to top. Figure 4-7(c) shows the magnitude to be approximately -1 dB. An element excited from top to bottom would have magnitude approximately -9 dB as given at theta equal 120°. The method described for separation of polarization depends on these values being equal in magnitude and 180° out of phase. The magnitudes for the 30° elevation angle are quite different and cancellation of the theta components of combined voltages would be far from complete. It is apparent then that the application of this method of polarization separation for elevation angles much higher than the horizon requires elevation plane patterns which are symmetric about the horizon.

Figure 4-7 displays another characteristic of the theta components of the far electric field. At 750 and 500 MHz, some deep nulls appear for various small elevation angles. These nulls cast some doubt on

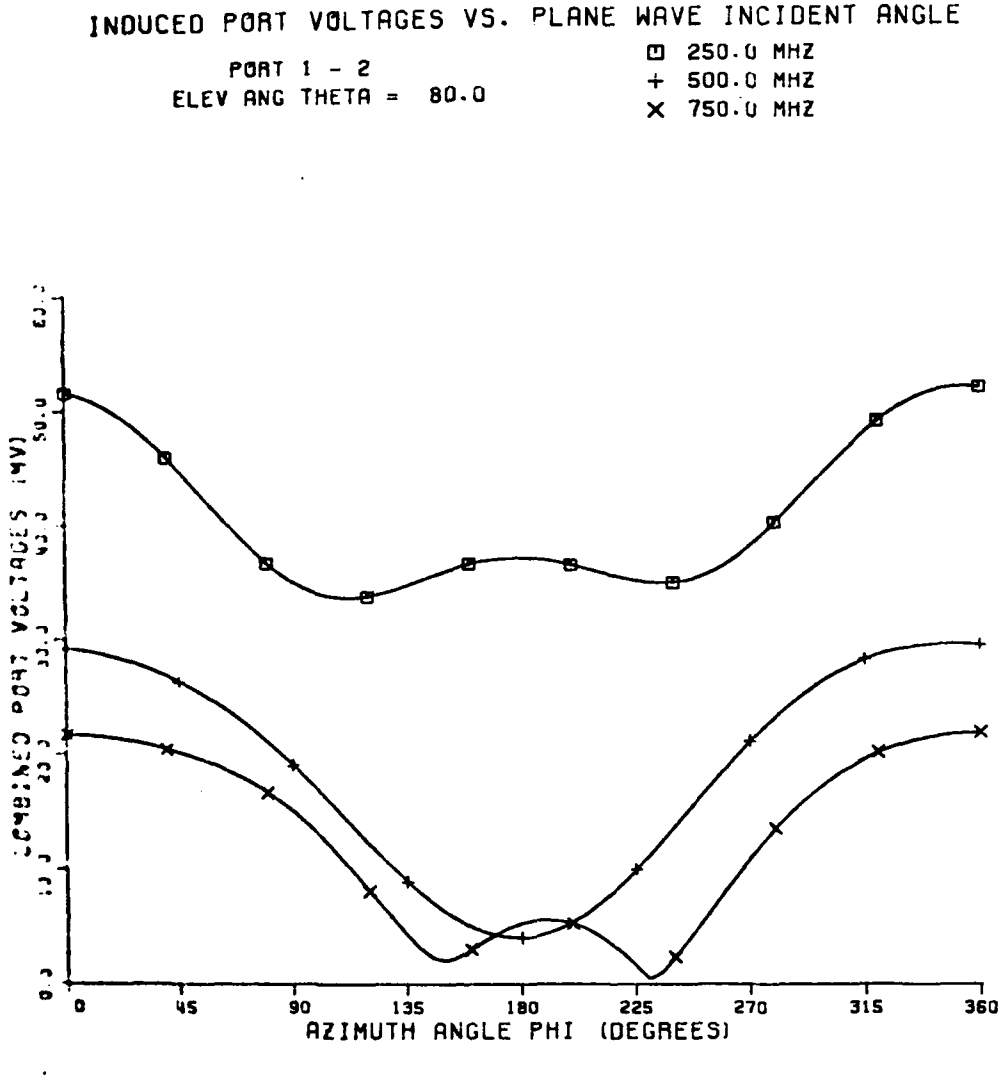

Fig. 4-5(a). Theta component of received voltage pattern obtained by subtracting voltage at Port 1 from Port 2. Three frequencies are shown. The incident wave is 10° above horizontal plane. The half-loop elements are on the finite cylinder.

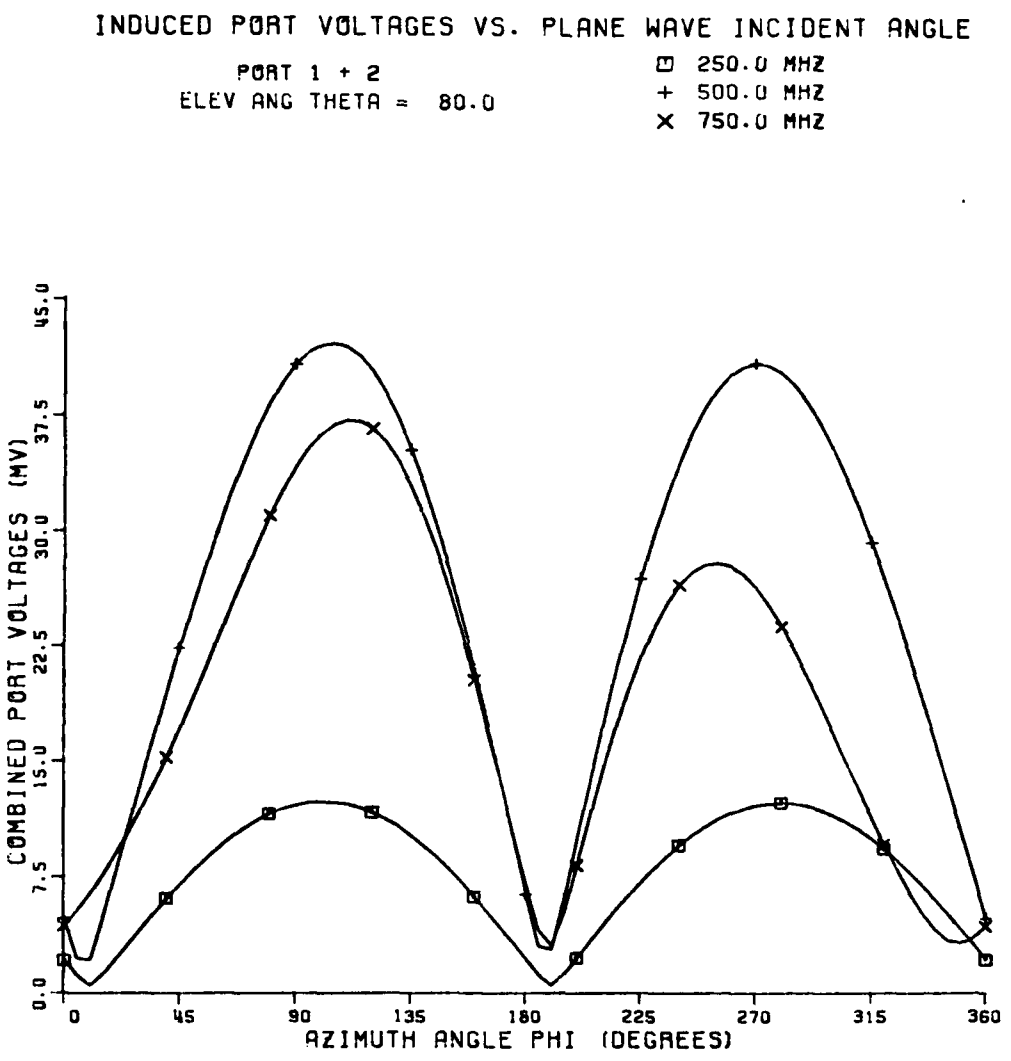

Fig. 4-5(b). Phi component of received voltage pattern obtained by adding voltage at Port 1 and Port 2. Three frequencies are shown. The incident wave is 10° above horizontal plane. The half-loop elements are on the finite cylinder.

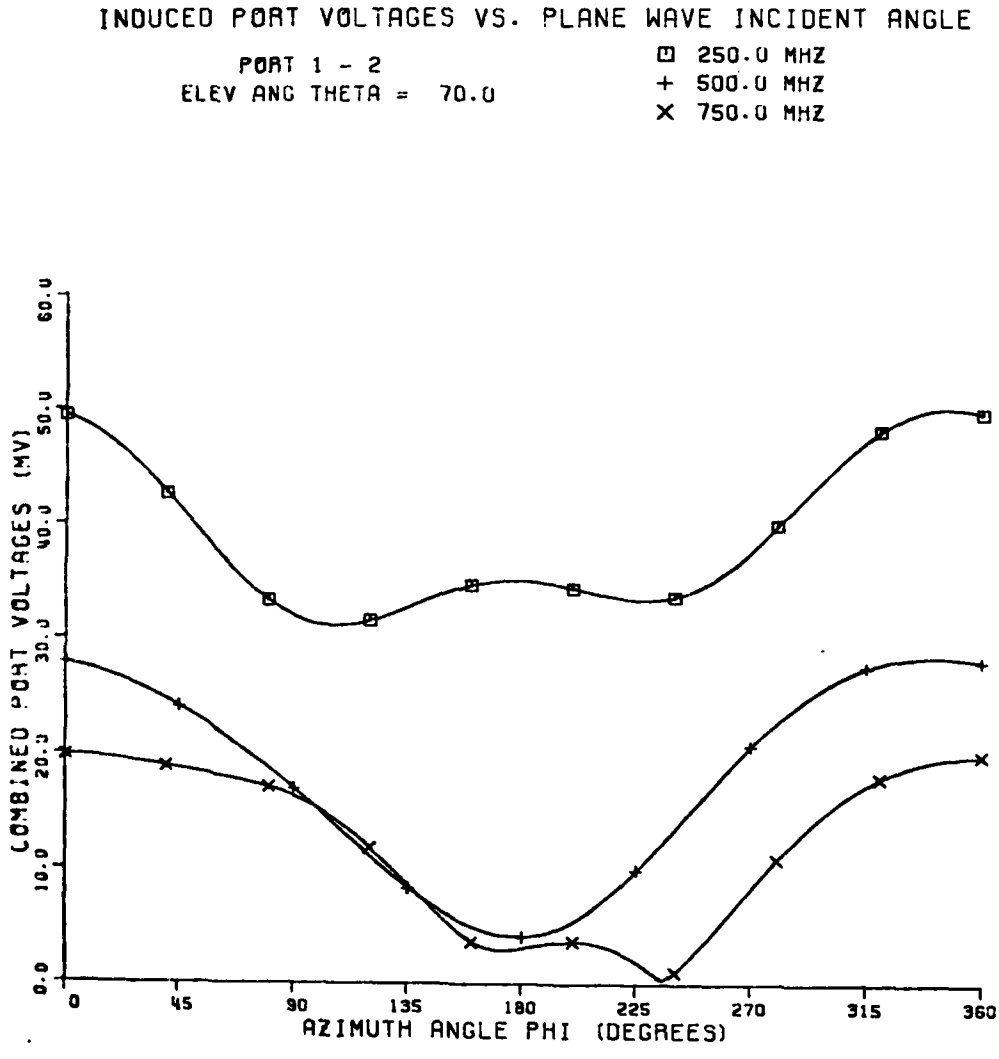

Fig. 4-6(a). Theta component of received voltage pattern obtained by subtracting voltage at Port 1 from Port 2. Three frequencies are shown. The incident wave is 20° above horizontal plane. The half-loop elements are on the finite cylinder.

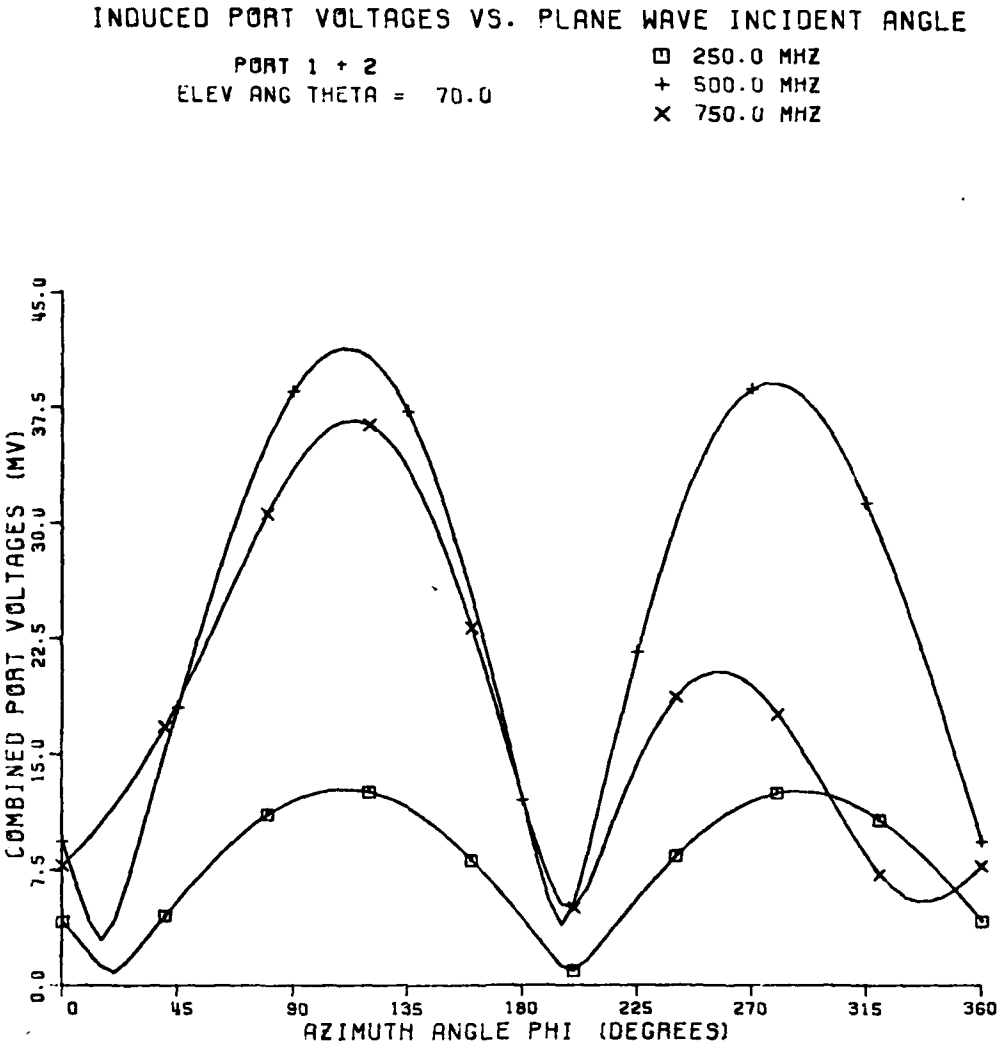

Fig. 4-6(b). Phi component of received voltage pattern obtained by adding voltage at Port 1 and Port 2. Three frequencies are shown. The incident wave is 20° above horizontal plane. The half-loop elements are on the finite cylinder.

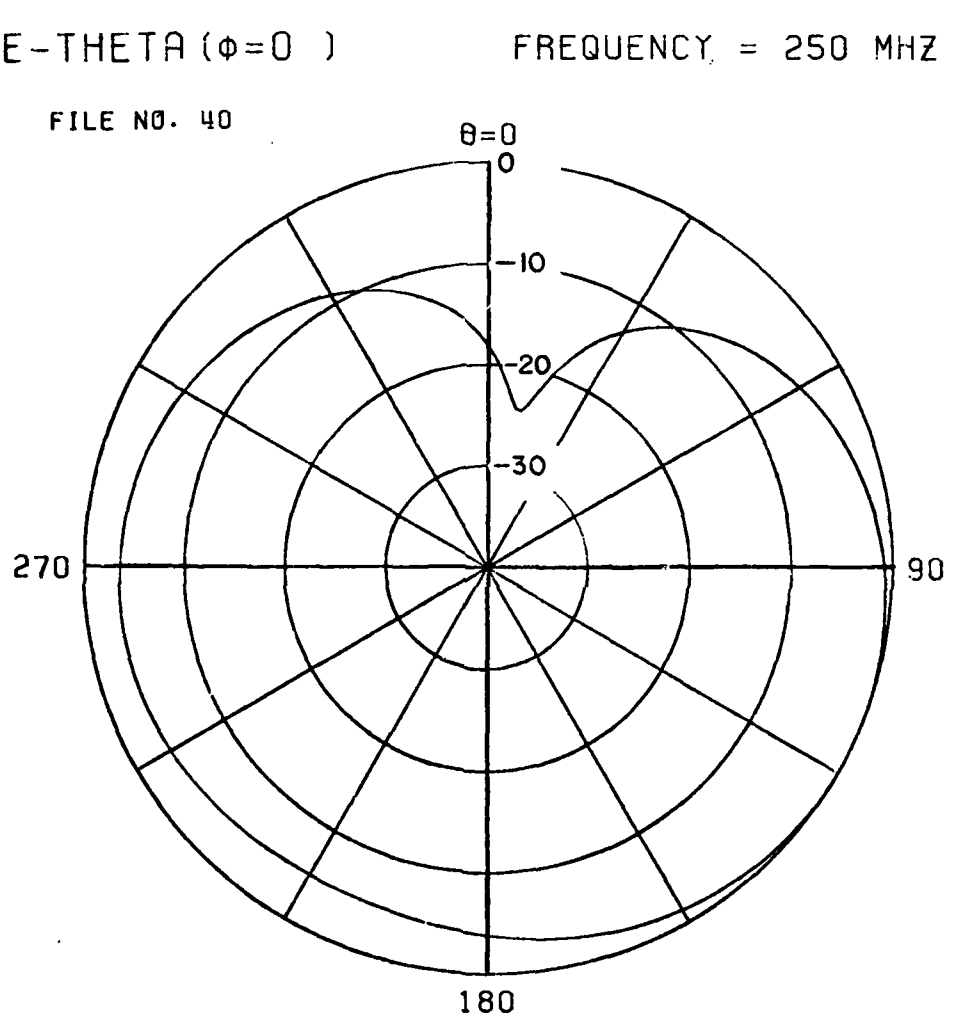

Fig. 4-7(a). Theta component of the far electric field pattern in the vertical plane for Port 1 half-loop of Fig. 4-3 located on the finite cylinder at a frequency of 250 MHz.

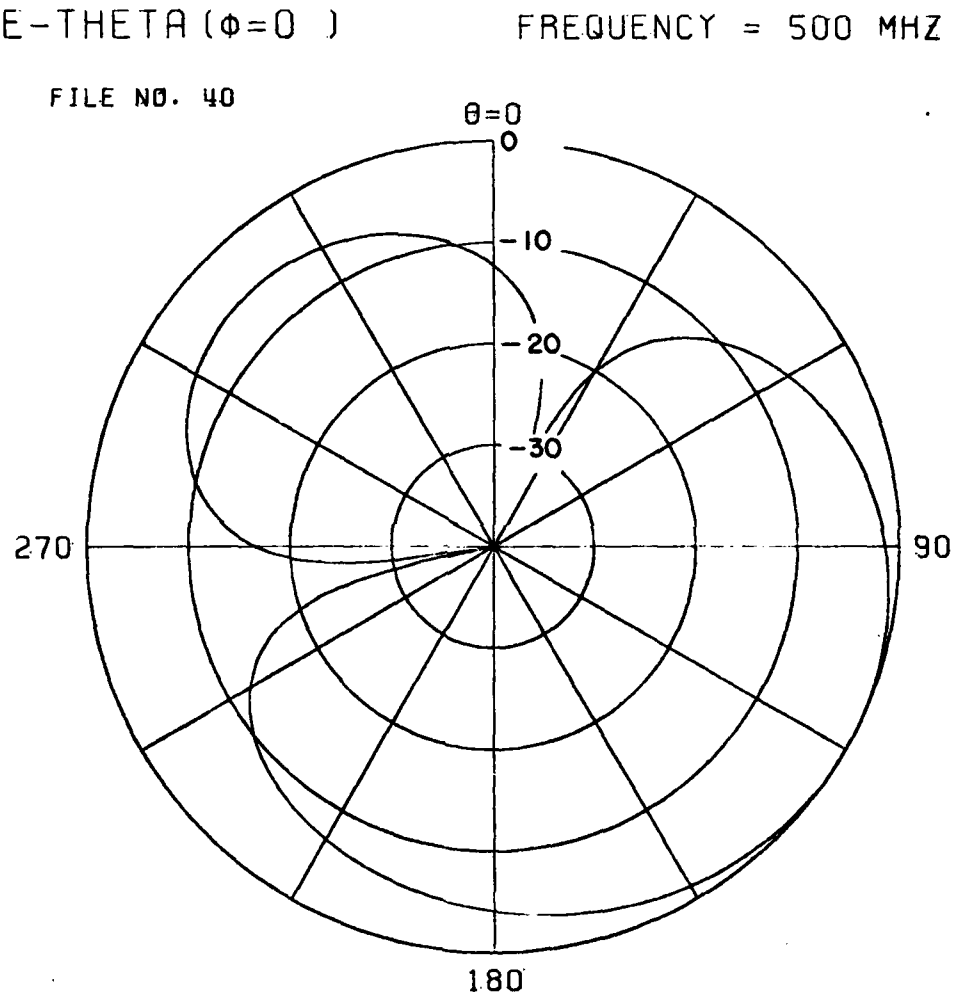

Fig. 4-7(b). Theta component of the far electric field pattern in the vertical plane for Port 1 half-loop of Fig. 4-3 located on the finite cylinder at a frequency of 500 MHz.

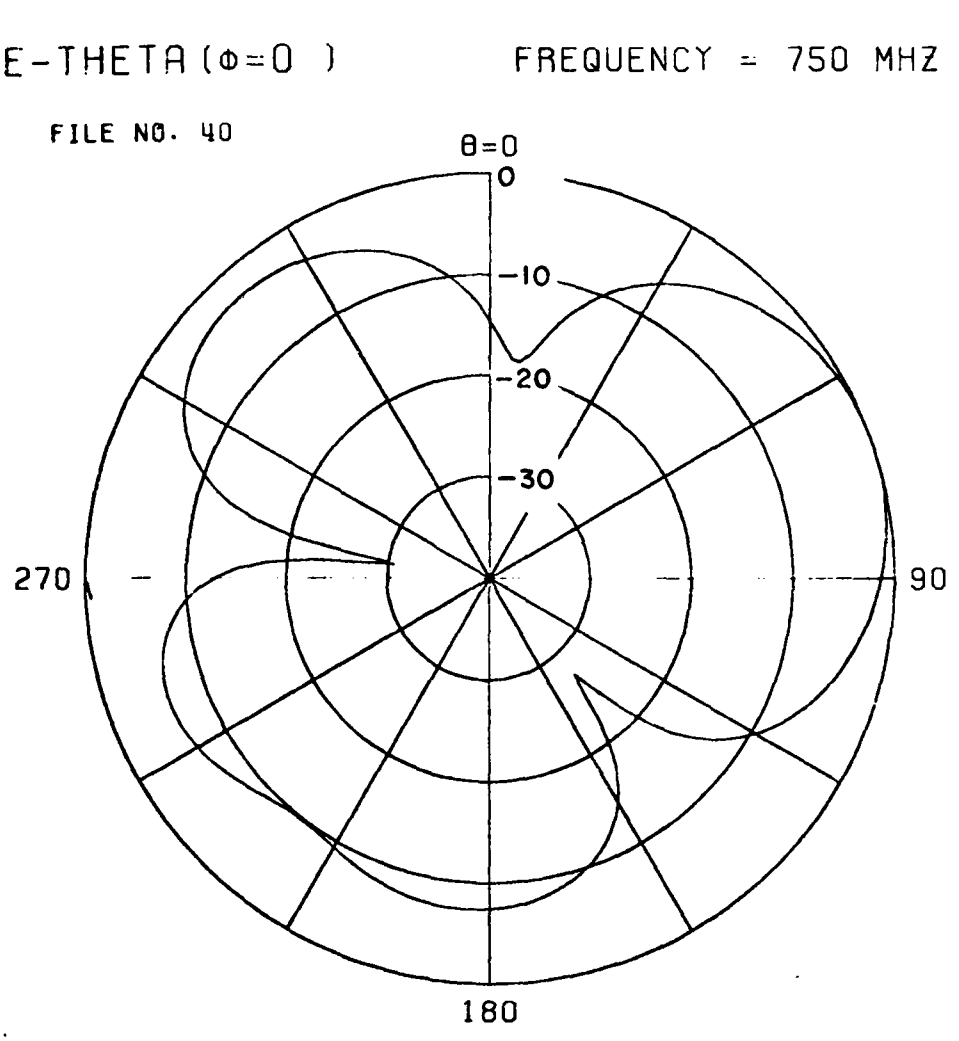

Fig. 4-7(c). Theta component of the far electric field pattern in the vertical plane for Port 1 half-loop of Fig. 4-3 located on the finite cylinder at a frequency of 750 MHz.

the practical value of the method, since deep pattern nulls can be very sensitive to environmental effects in a practical system. Small variation of the null angles could reduce the stability of the front-to-back ratio in the horizontal plane.

An investigation of the effects of the finite length of the cylinder shows that the main source of these deep nulls is the chosen length of the cylinder. The half-loop radiator and various other elements were analyzed in the presence of an infinite cylinder by the methods of Chapter III. The current distribution of the radiating element is first calculated by the moment method of Chapter II. This segmented distribution is then used to weight an infinitesimal radiator whose fields are calculated in the presence of the infinite cylinder. By the principle of superposition, these fields are summed to give the far-field pattern of the radiator on the infinite cylinder.

Figure 4-8 shows some results of applying this technique to the half-loop located on a cylinder of infinite length with diameter the same as the previous model. Comparing these patterns with Fig. 4-7 shows the effects of the finite cylinder length on the theta component of far electric field in the elevation plane. The deep nulls near the azimuthal plane have vanished over the frequency range, but the desired symmetry about the horizon is only slightly improved. An improvement in front-to-back ratio, especially at the lowest frequency is also apparent.

To relate these field patterns for an infinite cylinder to the induced voltage patterns of the input ports of Fig. 4-3, reciprocity may be employed. The theta and phi components of the far electric field for a half-loop fed from bottom to top are calculated and simply multiplied by a scale factor to become components of Port 1 voltage. Similarly, fields from a half-loop fed from top to bottom become components of Port 2 voltage. These port voltages may be processed as described previously in this section to separate the polarizations.

Results for elevation angles of 0°, 10°, 20° are shown in Figs. 4-9 through 4-11. Comparison of these results near an infinite cylinder with those of Figs. 4-4 through 4-6 for the finite length cylinder demonstrate the effects of the finite cylinder. The theta components of the induced port voltages have a larger front-to-back ratio and remain more constant over the frequency range and the range of elevation angles for the infinite cylinder case. The phi components of induced port voltages are only slightly more stable for the infinite cylinder case.

Thus, this section has demonstrated the method of separation of polarization of the incoming signal as applied to a half-loop radiator. The desired DF patterns of Section B have been duplicated over approximately a three-to-one frequency band for an arbitrarily polarized

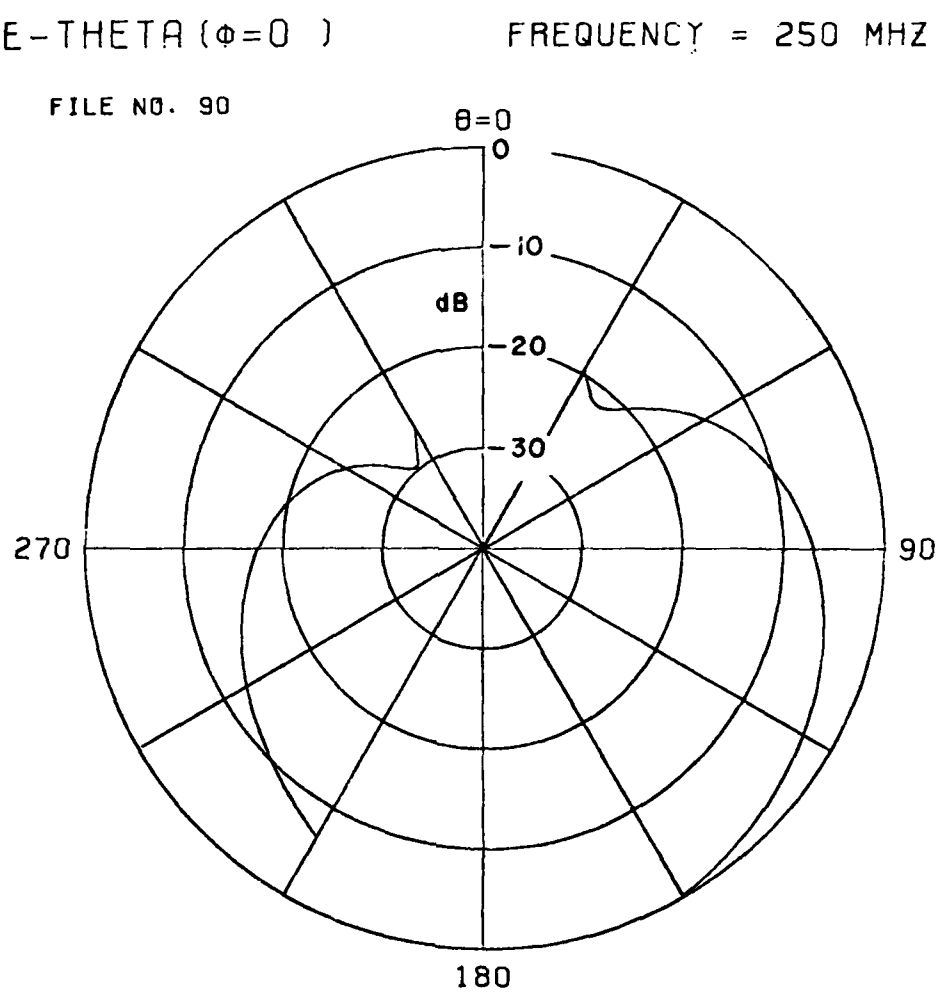

Fig. 4-8(a). Theta component of the far electric field pattern in the vertical plane for Port 1 half-loop of Fig. 4-3 located on the infinite cylinder at a frequency of 250 MHz.

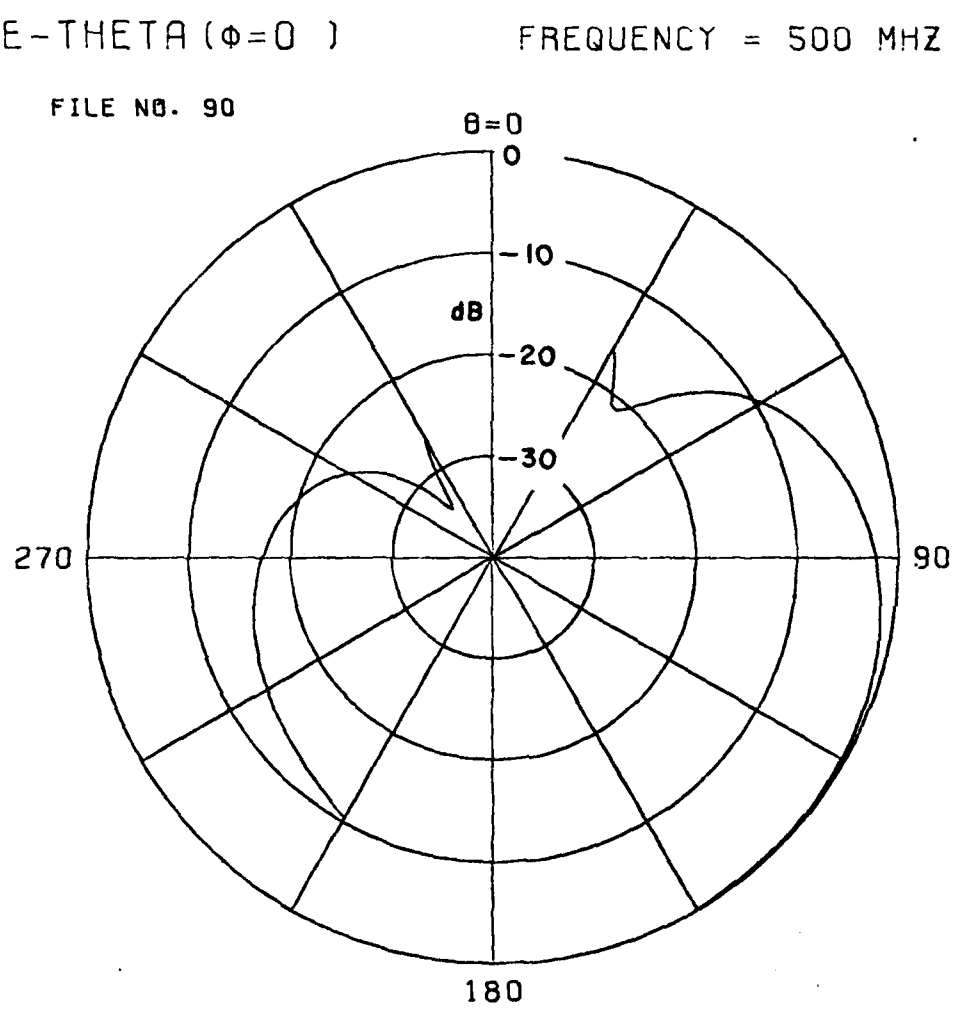

Fig. 4-8(b). Theta component of the far electric field pattern in the vertical plane for Port 1 half-loop of Fig. 4-3 located on the infinite cylinder at a frequency of 500 MHz.

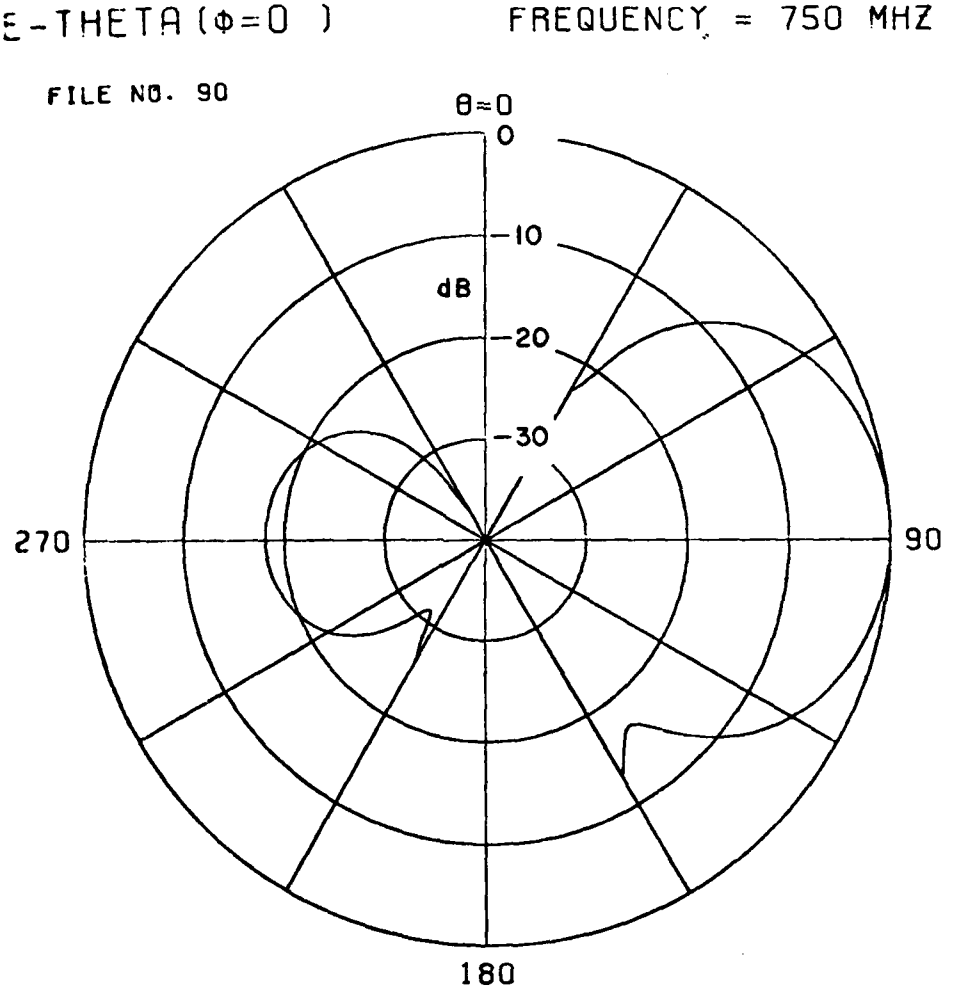

Fig. 4-8(c). Theta component of the far electric field pattern in the vertical plane for Port 1 half-loop of Fig. 4-3 located on the infinite cylinder at a frequency of 750 MHz.

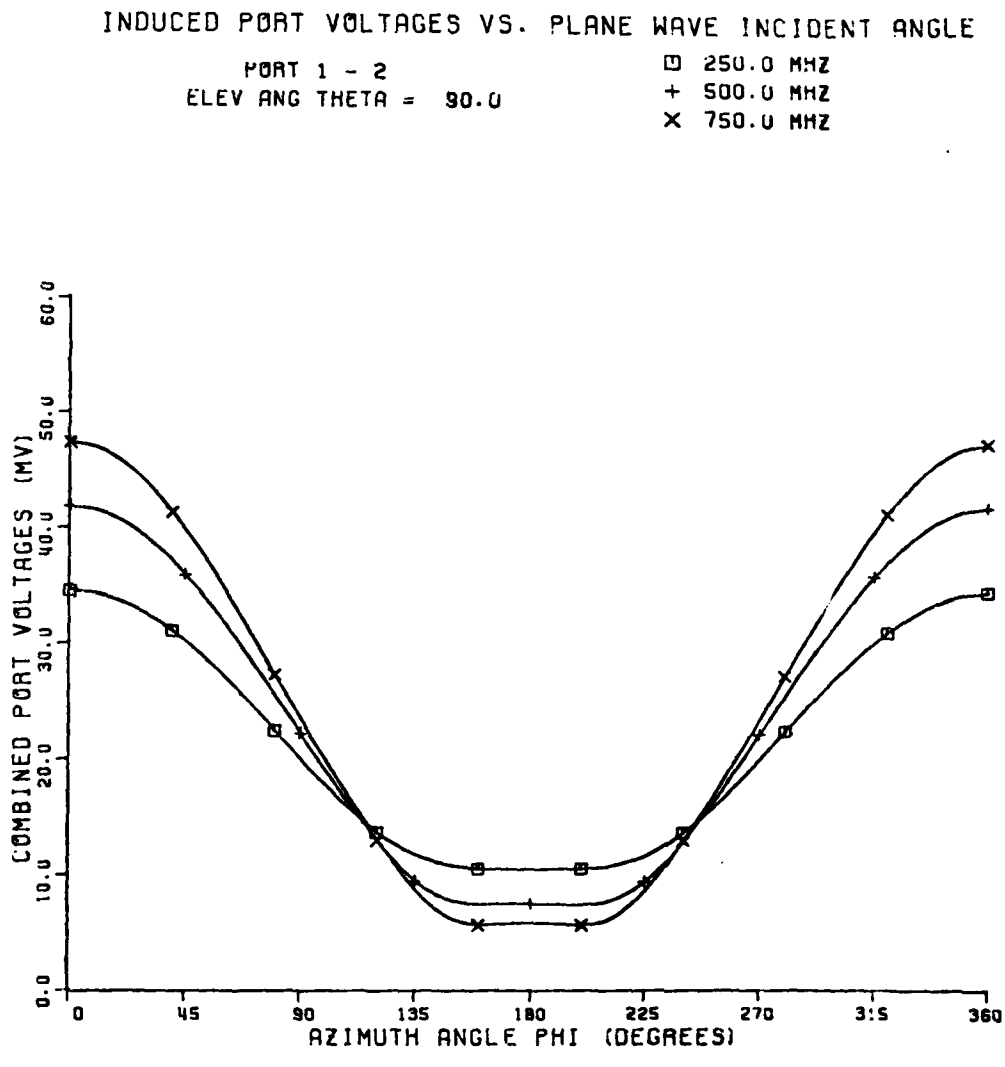

Fig. 4-9(a). Theta component of received voltage pattern obtained by subtracting voltage at Port 1 from Port 2. Three frequencies are shown. The incident wave is in the horizontal plane. The half-loop elements are on the infinite cylinder.

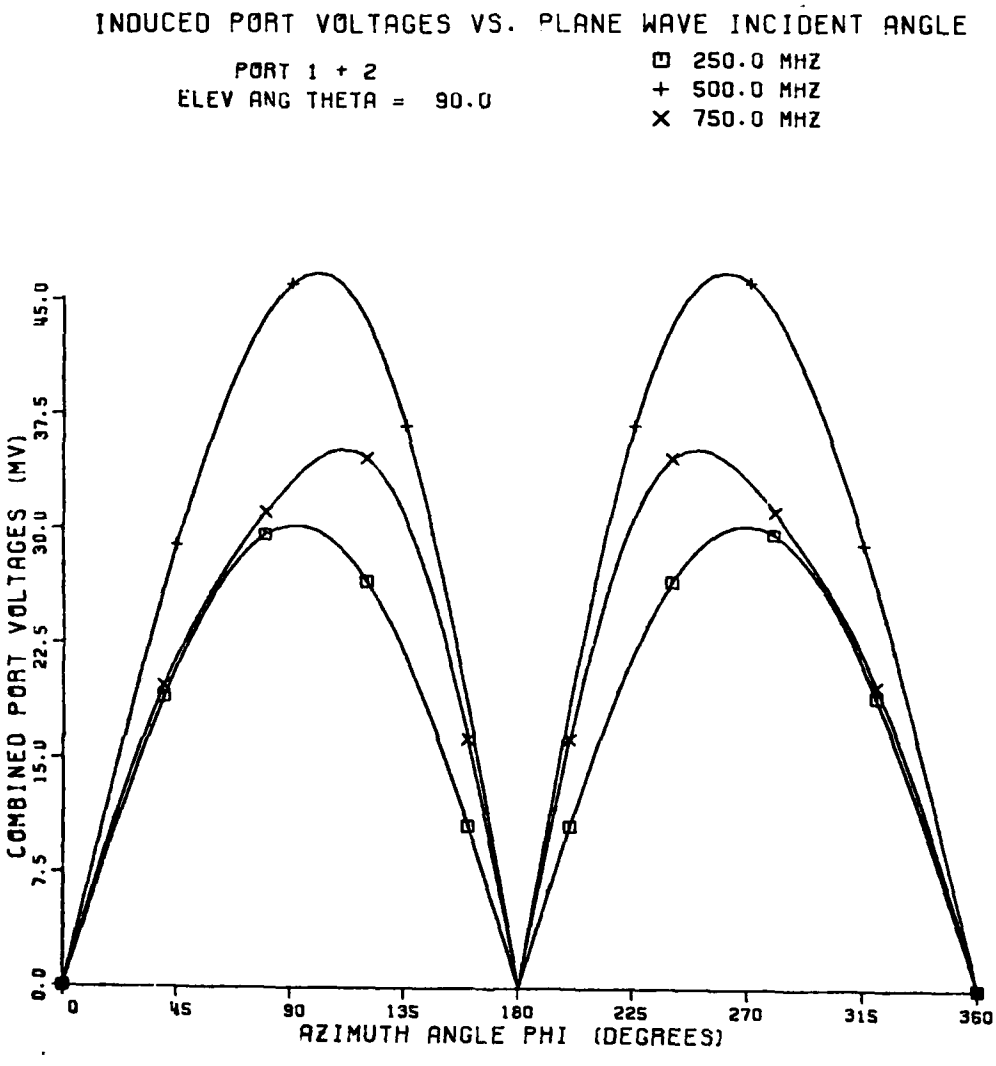

Fig. 4-9(b). Phi component of received voltage pattern obtained by adding voltage at Port 1 and Port 2. Three frequencies are shown. The incident wave is in the horizontal plane. The half-loop elements are on the infinite cylinder.

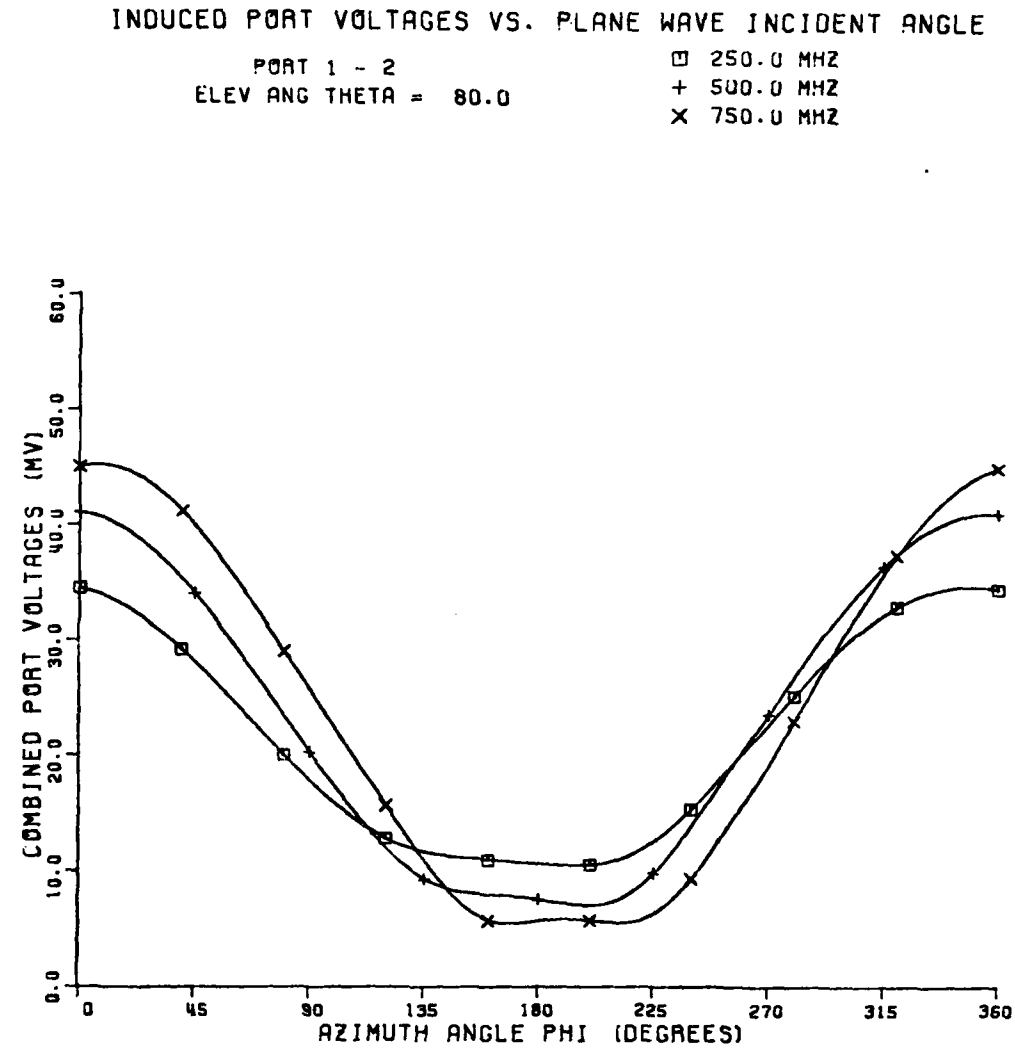

Fig. 4-10(a). Theta component of received voltage pattern obtained by subtracting voltage at Port 1 from Port 2. Three frequencies are shown. The incident wave is 10° above horizontal plane. The half-loop elements are on the infinite cylinder.

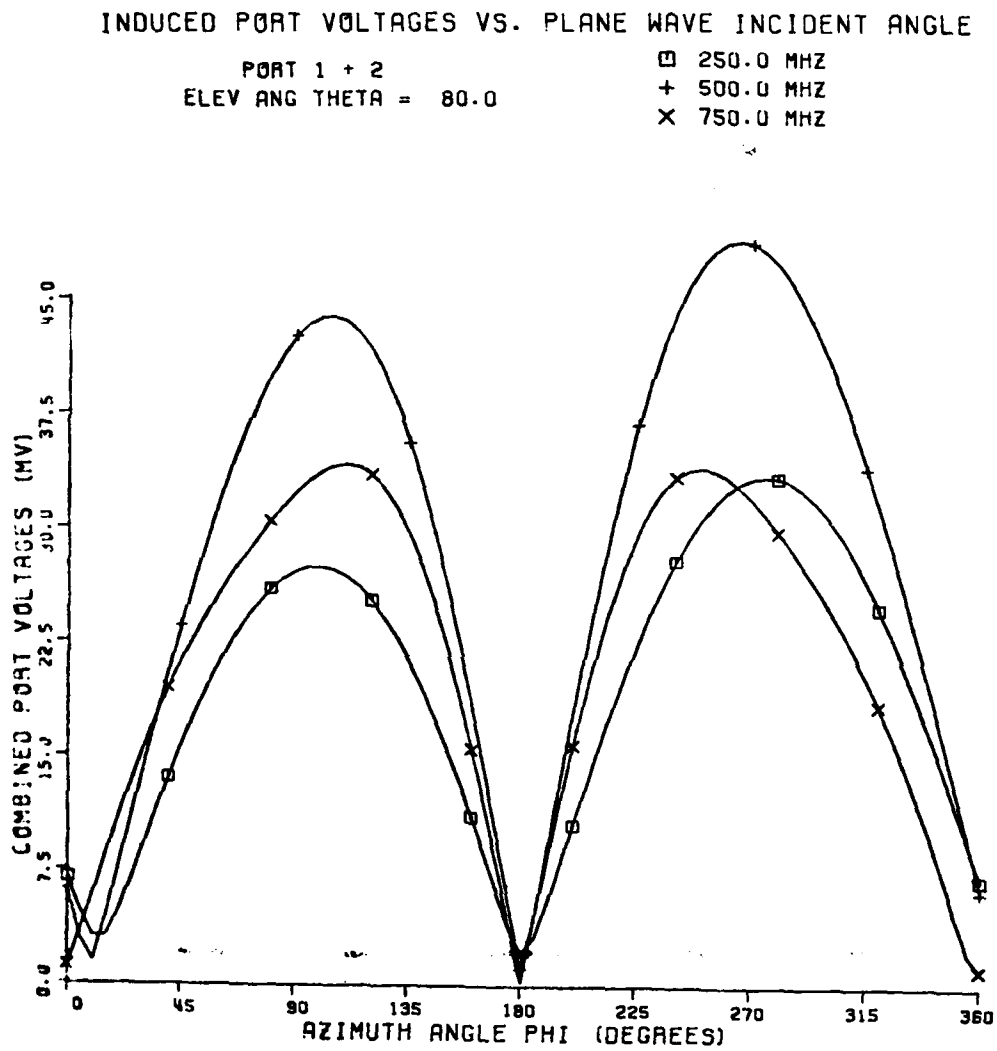

Fig. 4-10(b). Phi component of received voltage pattern obtained by adding voltage at Port 1 and Port 2. Three frequencies are shown. The incident wave is 10° above horizontal plane. The half-loop elements are on the infinite cylinder.

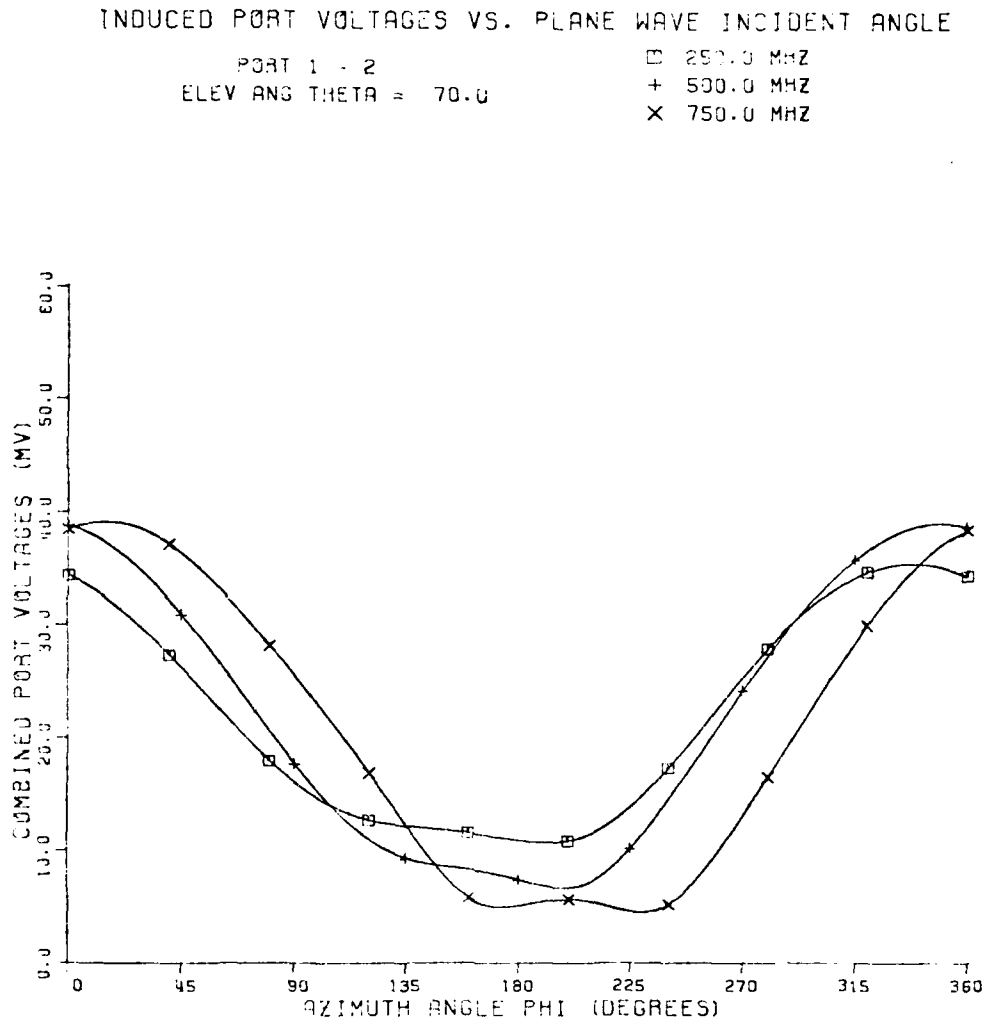

Fig. 4-11(a). Theta component of received voltage pattern obtained by subtracting voltage at Port 1 from Port 2. Three frequencies are shown. The incident wave is 20° above horizontal plane. The half-loop elements are on the infinite cylinder.

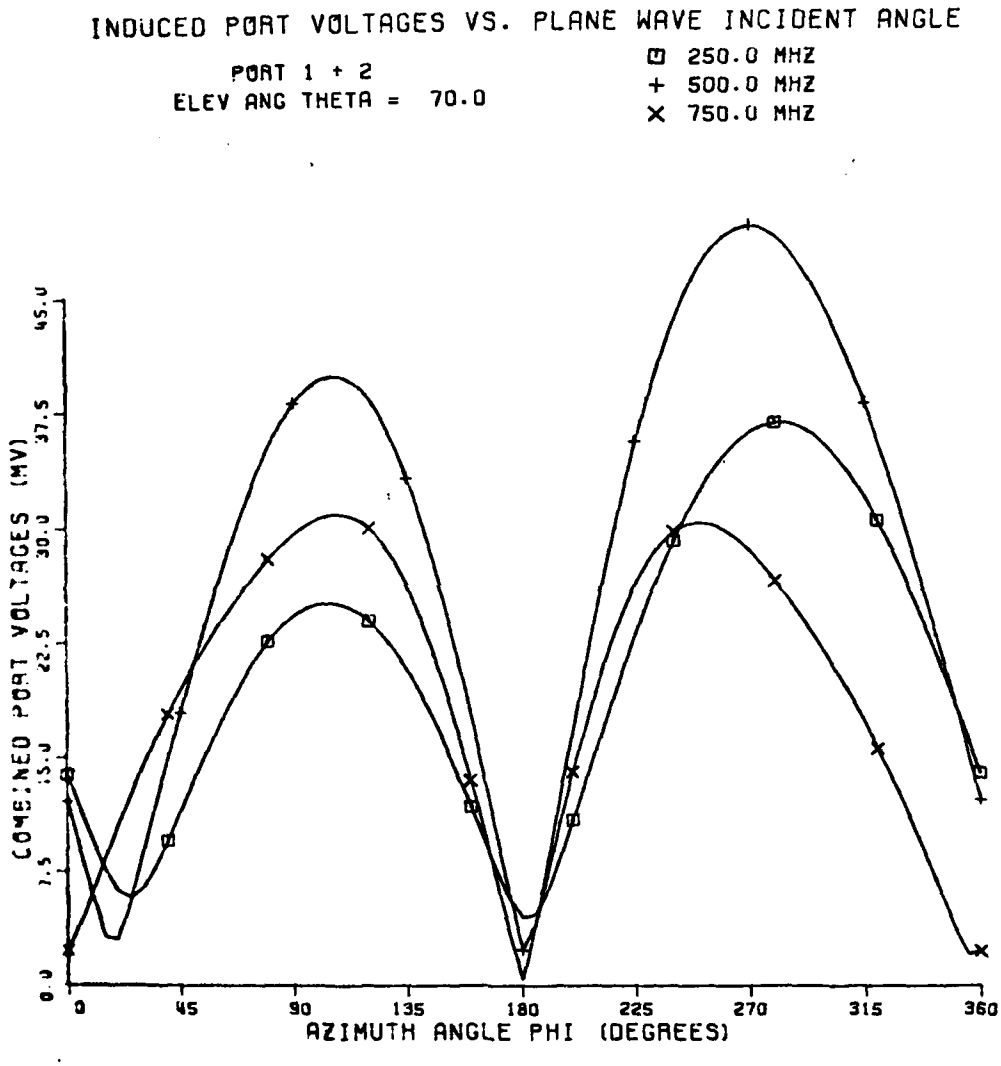

Fig. 4-11(b). Phi component of received voltage pattern obtained by adding voltage at Port 1 and Port 2. Three frequencies are shown. The incident wave is 20° above horizontal plane. The half-loop elements are on the infinite cylinder.

incident signal in or near the azimuthal plane. The method is presently limited to small elevation angles because of asymmetries in the elevation plane patterns of the half-loop radiator in the presence of the cylinder. Comparison of results obtained for a finite length cylinder with those of an infinite length cylinder shows better results when the cylinder is electrically long.

F. Input Impedance and Radiation Efficiency

An important consideration for any antenna, transmitting or receiving, is the power loss involved in the transfer of energy via the antenna. Conventionally, this loss is divided into two quantities. One is mismatch loss, measured as VSWR, due to the antenna input impedance being unequal to the impedance of the connecting line or cable. The second is radiation efficiency due to losses in the antenna element itself such as omhic losses. For the electrically small radiators considered in this study, a trade-off between antenna efficiency and VSWR was clearly established.

A direction finding system would be most concerned with antennas utilized in the receiving mode. Radiation efficiency of a receiving antenna can usually be considerably lower than for a transmitting antenna. Extensive investigation of antenna input impedance versus antenna efficiency was conducted on various electrically small radiators. Perfectly-conducting radiating elements tend to have highly resonant input impedances. That is, the input impedance varies rapidly over a frequency band. The corresponding VSWR also changes rapidly and can be quite large, even over a small frequency range. Introducing loss into the radiator in the form of reduced conductivity or lumped loads connected with perfectly-conducting segments damps the rapidly varying input impedance. Thus, radiators formed from lossy wires or wires which are loaded, provide a means for stabilizing the input impedance and correspondingly the VSWR. This improvement is made at the expense of antenna efficiency. Resistive losses due to the decreased conductivity or lumped loads greatly reduce the antenna efficiency. Various loading schemes were investigated on numerous radiating elements; however, this paper will present results for only one loading scheme as applied to half-loop radiators of Fig. 4-3. The method used a tapered distribution [7] of lumped resistive loads of values shown in the figure. These values are not picked to optmize any particular parameter, but to demonstrate the possibilities proper loading can offer in terms of mismatch versus radiation efficiency. Figure 4-12 shows a Smith Chart mapping the input impedance over a four-to-one frequency band when normalized to 300 Ω. The VSWR remains below 1.65. Table 4-1 shows the corresponding antenna efficiencies for this frequency range.

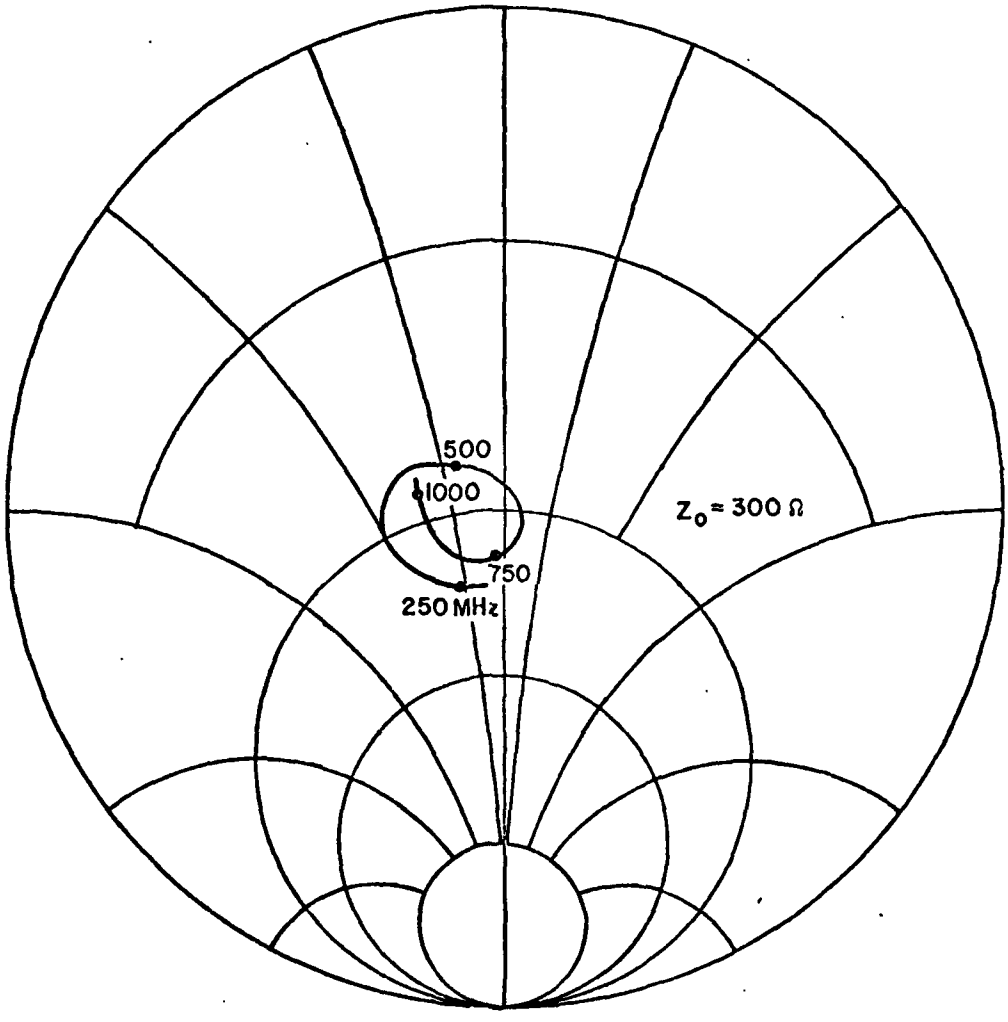

Fig. 4-12. Smith chart plot of input impedance of half-loop element of Fig. 4-3 on a finite cylinder. The input impedance is normalized to 300Ω .

TABLE 4-1

Frequency	Efficiency	Input Impedance
250 MHz	4.27%	(402.0 - j63.2)Ω
500 MHz	17.10%	(236.9 - j42.8)Ω
750 MHz	25.40%	(368.2 - j10.7)Ω
1000 MHz	36.50%	(256.4 - j101.1)Ω

CHAPTER V

SUMMARY AND CONCLUSIONS

To summarize, a method of direction finding has been proposed and demonstrated. The method evolved in the process of surmounting the constraints of the problem. The antenna radiating elements were to be electrically small and located on a cylinder whose electrical dimensions were larger. This caused the component field pattern shapes and directivity to be limited to two basic kinds: the figure eight phi pattern and the broad single lobed theta pattern. When considered independently, these patterns were shown to be capable of direction finding; however, practical elements investigated induced both simultaneously. By correctly combining properly oriented radiators, the independent patterns were recovered for arbitrarily polarized DF signals in or near the azimuthal plane.

Further, the system was to perform over a broad frequency range with the frequency of the incident signal unknown. Processing of the incoming signals was to be of the most elementary kind, that is, a simple processing algorithm was to work for all signals in the operating band. These constraints required that the pattern shapes, including the location of maxima and minima, remained constant over the frequency band. These necessary requirements were achieved and demonstrated for a particular radiating element over a three-to-one frequency band.

An antenna system operating over a frequency range has the added difficulty of maintaining a reasonably well-behaved input impedance so that mismatch losses are minimized. Perfectly-conducting radiators of the type investigated have rapidly varying input impedances over the frequency band. A method of tapered loading has been demonstrated which effectively damps this variation at the sacrifice of antenna efficiency. Thus, a method using electrically small radiators properly formed into an array around a cylinder has been demonstrated to be capable of direction finding over a frequency band with minimal signal processing, even when the frequency, phase and polarization of the incoming signal are unknown.

The investigation of the DF system was facilitated by the use of modern numerical techniques in antenna analysis. Radiating elements in the presence of the cylinder were analyzed using two approximate techniques. One was a specialized moment method in

which the antenna structure was wire-grid modeled, and piecewise-sinusoidal expansion and weight functions were assumed and reaction enforced. This method was applied to radiators on finite cylinders. The second method was a hybrid technique which used currents calculated by the first method to weight infinitesimal elements near an infinite cylinder whose far fields were found by modal solutions. Integration over the element apertures gave the total fields. The accuracy of the wire-grid modeling method has been well documented in the literature. The second method uses exact equations for the fields, the approximation being the weighting factor calculated from a discrete current distribution generated on a finite cylinder. The accuracy of this method is very good when the elements are loaded and sufficient current samples are used over the element.

Several limitations of the specific radiator chosen to demonstrate the DF system concept were discussed. The half-loop's phi component of electric field in horizontal plane had a maximum which drifted slightly over the frequency range. The theta component of electric field in the elevation plane was asymmetric about the horizon, causing the polarization separation technique to work for only small angles of elevation. These limitations for this particular radiator do not preclude the use of this concept for systems which need a broader bandwidth or higher elevation angles. A radiating element would need to be designed with more symmetric elevation plane patterns and less pattern shift over a larger frequency bandwidth.

Results of the investigations of small radiators on the conducting cylinder suggest several topics for further research. First, a search for a practical radiating element which is sensitive to phi polarized signals and blind to theta components should be completed. One possible candidate is a small loop located in the horizontal plane. Elements with more symmetric elevation plane patterns could be utilized to extend the method for higher elevation angles. Design curves could be calculated so that for given loss specifications an optimum mismatch versus efficiency trade-off could be obtained for various loading schemes. Finally, experimental verification of the computer calculated results should be carried out. This would be especially desirable and satisfying for a system whose specifications are fixed, including frequency bandwidth, tolerable power loss, necessary accuracy, and conformal geometry constraints.

REFERENCES

1. J. H. Richmond, "Computer Program for Thin Wire Structures in a Homogeneous Conducting Medium," Report 2902-12, August 1973, The Ohio State University ElectroScience Laboratory, Department of Electrical Engineering; prepared under Grant NGL 36-008-138, for the National Aeronautics and Space Administration, Langely Research Center, Hampton, Virginia, pp. 1-50.

2. P. K. Agrawal, G. A. Richards, G. A. Thiele, J. H. Richmond, "Analysis and Design of TEM-Line Antennas," IEEE Transactions on Antennas and Propagation, Vol. AP-20, No. 5, September 1972.

3. G. A. Thiele, "Wire Antennas," Chapter 2 of Computer Techniques for Electromagnetics, Vol. 7, R. Mittra (Ed.), Pergamon Press, Oxford and New York, 1973.

4. Burnside, W. D., "Analysis of On-Aircraft Antenna Patterns," Report 3390-1, August 1972, The Ohio State University ElectroScience Laboratory, Department of Electrical Engineering; prepared under Contract N62269-72-C-0354 for Naval Air Development Center. (AD 777 989)

5. G. Sinclair, "The Patterns of Antennas Located Near Cylinders of Elliptical Cross Section," Proceedings IRE, Vol. 39, No. 6, June 1951.

6. J. H. Richmond (private communication).

7. E. Burvin (private communication).